DISSERTATIONES
PHYSICAE
UNIVERSITATIS
TARTUENSIS
101

KAAREL PIIP

Development of LIBS for *in-situ* study of ITER relevant materials

DISSERTATIONES PHYSICAE UNIVERSITATIS TARTUENSIS

101

DISSERTATIONES PHYSICAE UNIVERSITATIS TARTUENSIS
101

KAAREL PIIP

Development of LIBS for *in-situ* study of ITER relevant materials

UNIVERSITY OF TARTU
Press

This study was carried out at the University of Tartu.

The dissertation was admitted on 05.04.2016 in partial fulfilment of the requirements for the degree of Doctor of Philosophy in Physics, and was allowed for defence by the Council of the Institute of Physics, University of Tartu.

Supervisors: Assoc. Prof. Matti Laan, University of Tartu, Estonia
PhD Peeter Paris, University of Tartu, Estonia

Opponent: PhD Pavel Veis, Comenius University in Bratislava, Bratislava, Slovakia

Defence: June 16, 2016, at the University of Tartu

The research presented in this thesis is supported by the Estonian Science Foundation project no. ETF9310, targeted funding project SF0180051s12, EUROfusion project MLOFY14130, and graduate school "Functional materials and technologies".

ISSN 1406-0647
ISBN 978-9949-77-113-4 (print)
ISBN 978-9949-77-114-1 (pdf)

University of Tartu Press
www.tyk.ee

CONTENTS

LIST OF THE PUBLICATIONS INCLUDED IN THE THESIS 7

LIST OF ABBREVIATIONS, NOTATIONS AND ACRONYMS 9

INTRODUCTION 10

CHAPTER 1: THEORETICAL BACKGROUND 11
1.1. Laser-induced breakdown spectroscopy (LIBS) 11
1.1.1. The main idea 11
1.1.2. Dynamics of the laser-induced plasma 12
1.1.3. Basic processing of the LIBS spectra 14
1.1.4. Data processing: elemental depth profiles and averaging 15
1.1.5. Calibration free LIBS (CF-LIBS): idea and requirements 16
1.1.6. Boltzmann diagrams 16
1.1.7. Local thermodynamic equilibrium (LTE) 17
1.2. Plasma surface interaction (PSI) 18
1.2.1. General considerations 18
1.2.2. Results of ITER-relevant materials studies 19
1.2.3. LIBS as a method for monitoring PSI processes: results, current problems and limitations 20

CHAPTER 2: EXPERIMENTAL 21
2.1. Setup 21
2.1.1. Domestic LIBS setup 21
2.1.2. Linear plasma machines Pilot-PSI and Magnum-PSI 22
2.1.3. Additional surface characterization methods 25
2.2. Samples 26

CHAPTER 3: RESULTS AND DISCUSSION 28
3.1. Characterization of ITER-relevant materials by time resolved LIBS 28
3.1.1. Ablation regularities at low (10^{-3} mbar) pressure and 1–2 mbar Ar background pressure 28
3.1.2. Selection of W spectral lines 30
3.1.3. Tests on virgin W coatings 31
3.1.4. D detection from W and W/Al mixture coated samples 35
3.2. Experiments on samples exposed to plasma 37
3.2.1. Experiments on W coatings exposed to Pilot-PSI He and D plasma 37
3.2.2. Tests on samples exposed to linear plasma devices and AUG plasma 40
3.3. *In-situ* LIBS measurements on linear plasma devices 40
3.3.1. *In-situ* LIBS system development on Magnum-PSI 40
3.3.2. *In-situ* LIBS measurements on Pilot-PSI 41

SUMMARY (MAIN RESULTS) 48

OPEN PROBLEMS AND SUGGESTIONS FOR THE FURTHER RESEARCH 50
SUMMARY IN ESTONIAN 51
ACKNOWLEDGEMENTS 54
REFERENCES 55
PUBLICATIONS 59
CURRICULUM VITAE 85
ELULOOKIRJELDUS 87

LIST OF THE PUBLICATIONS INCLUDED IN THE THESIS

[I] Lissovski, A.; **Piip, K**.; Hämarik, L.; Aints, M.; Laan, M.; Paris, P.; Hakola, A.; Karhunen, J. (2015). LIBS for tungsten diagnostics in vacuum: Selection of analytes. *Journal of Nuclear Materials*, 463, 923−926

[II] **Piip, K**.; De Temmerman, G.; van der Meiden, H.J.; Lissovski, A; Karhunen, J.; Aints, M.; Hakola, A.; Paris, P.; Laan, M.; Likonen, J.; Jõgi, I.; Kozlova, J.; Mändar, H. (2015). LIBS analysis of tungsten coatings exposed to Magnum PSI ELM-like plasma. Journal of Nuclear Materials, 463, 919−922,

[III] **Piip, K**.; Paris, P.; Hakola, A.; Bystrov, K.; De Temmerman, G.; Aints, M.; Jõgi, I.; Kozlova, J.; Laan, M.; Likonen, J.; Lissovski, A.; Mändar, H. (2014). Influence of He/D_2 plasma fluxes on the morphology and crystallinity of tungsten coatings. Physica Scripta, 89 (4), nr 044009

[IV] Paris, P.; **Piip, K**.; Hakola, A.; Laan, M.; Aints, M.; Koivuranta, S.; Likonen, J.; Lissovski, A.; Mayer, M.; Neu, N.; Rohde, V.; Sugiyama, K. (2015). Development of laser induced breakdown spectroscopy for studying erosion, deposition, and fuel retention in ASDEX Upgrade. Fusion Engineering and Design, 98–99, 1349−1352

Author's contribution

[I] Performing the LIBS measurements and active participation in the preparation of the manuscript.

[II] Planning the experiments, installing LIBS setup to the Magnum-PSI device and carrying out the experiments (in collaboration with DIFFER institute scientists), participation in data analyzes and preparation of the manuscript.

[III] Participation in the measurements, analyzing the data and preparation of the manuscript.

[IV] Participation in the measurements, analyzing the data.

Other related publications

[a] Karhunen, J.; Hakola, A.; Likonen, J.; Lissovski, A.; Paris, P.; Laan, M.; **Piip, K**.; Porosnicu, C.; Lungu, C. P.; Sugiyama, K. (2014). Development of laser-induced breakdown spectroscopy for analyzing deposited layers in ITER. Physica Scripta, 2014, 014067

[b] Van der Meiden, H.; Berg, M.; Brons, S.; Ding, H.; Eck, H.; Hoen, M.; Karhunen, J.; Kruif, T.; Laan, M.; Li, C.; Lissovski, A.; Morgan, T.; Paris, P.; **Piip, K.**; Pol, M.; Scannell, R.; Scholten, J.; Smeets, P.; Spork, C.; Emmichoven, P. ... De Temmerman, G. (2013). Laser-based diagnostics applications for plasma-surface interaction studies. Journal of Instrumentation, 8, 1−14,

[c] **Piip, K**.; Van der Meiden, H. J.; Hämarik, L.; Karhunen, J.; Hakola, A.; Paris, P.; Aints, M.; Laan, M.; Likonen, J.; Bystrov, K.; Kozlova, J.;

Kanarbik, R. (2015). In situ LIBS in the linear plasma device Pilot-PSI for Fusion Application. *15th International Conference on Plasma Facing Materials & Components for Fusion Applications, Aix-en-Provence, 18–22 May, 2015.* 75−75, book of abstracts

[d] **Piip, K**.; Paris, P.; Hakola, A.; Bystrov, K.; De Temmerman, G.; Aints, M.; Jõgi, I.; Kozlova, J.; Laan, M.; Likonen, J.; Lissovski, A. (2013). Influence of He/D_2 plasma fluxes on tungsten marker coatings. *In: 14th International Conference on Plasma-Facing Materials and Components for Fusion Applications Book of Abstracts: 14th International Conference on Plasma-Facing Materials and Components for Fusion Applications, Juelich, Germany, 13–17 May 2013.*

[e] **Piip, K.**; Laan, M.; Paris, P.; Aints, M.; Hakola, A.; Karhunen, J.; Likonen, J.; Lissovski, A.; Petersson, P.; Rubel, M. (2013). First wall monitoring by LIBS: options and limitations. *In: Europhysics Conference Abstracts: 40th EPS Conference on Plasma Physics; Finland Espoo; 1–5 July.* (37D).

LIST OF ABBREVIATIONS, NOTATIONS AND ACRONYMS

Ar	argon
AUG	ASDEX Upgrade (tokamak)
Be	beryllium
CF-LIBS	calibration free laser-induced breakdown spectroscopy
D	deuterium
E	energy
Δt	time-gate
Φ	laser fluence
FWHM	full width at half maximum
H	hydrogen
He	helium
I	intensity
ICCD	intensified charge coupling device
IR	infrared
ITER	international thermonuclear experimental reactor (tokamak)
JET	joint European torus (tokamak)
λ	wavelength
LIAS	laser-induced ablation spectroscopy
LIBS	laser-induced breakdown spectroscopy
LIDS	laser-induced desorption spectroscopy
n_e	electron density
Ne	neon
NRA	nuclear reaction analyzes
PIXE	particle-induced X-ray emission
RBS	Rutherford back-scattering
SEM	scanning electron microscopy
SIMS	secondary ion mass-spectroscopy
SNR	signal-to-noise ratio
T	tritium
T_e	electron temperature
T_{exc}	excitation temperature
t_d	delay time
UV	ultraviolet
VIS	visible (light)
W	tungsten
XRD	X-ray diffraction

INTRODUCTION

Compared to the traditional ways of energy production, the using of nuclear fusion has several advantages [1]. ITER (**I**nternational **T**hermonuclear **E**xperimental **R**eactor) is a step on the way of application of new energy source. The first plasma in ITER is planned in 2020. A number of physical and engineering problems for ITER are solved, but there are still essential topics that need further study. Among these issues are the life-time of plasma-facing components and the fuel retention in reactor walls [2]. *Post-mortem* methods are not suitable for wall monitoring: only the cumulative effect of the plasma pulses could be measured, while ITER will reach in one pulse a particle fluence to the wall comparable to that of present large devices within about one operational year [2].

Laser based techniques are promising candidates for *in-situ* wall characterization. Laser based techniques such as laser-induced breakdown spectroscopy (LIBS), laser-induced desorption spectroscopy (LIDS) and laser-induced ablation spectroscopy (LIAS) need only optical access to the components tested.

Nevertheless, ITER relevant materials such as tungsten (W), are not well studied from the viewpoint of LIBS analysis. Before applying quantitative LIBS in real tokamak environment, properties such as ablation rate, self-absorption of the spectral lines etc. have to be carefully studied. Besides, a reliable detection of hydrogen isotopes and estimation of their concentrations needs further study.

The main goal of this study is to clarify the main regularities needed to apply LIBS as a quantitative *in*-situ tool for monitoring W-containing layers erosion in ITER and at least for qualitative fuel retention (deuterium) measurements. To obtain results applicable in ITER, the relation between the tungsten surface structures caused by ITER-relevant plasma fluxes and LIBS spectra characteristics is studied. To reach the main goal, a number of sub goals are set. Most important of these are the following: study of the tungsten laser-induced plasma dynamics; selection of tungsten spectral lines suitable for tungsten analyzes; detection of deuterium from tungsten samples; investigating the effect of the sample surface morphology to the LIBS spectra; installing *in-situ* LIBS system for linear plasma devices and carrying out material erosion and deuterium retention measurements.

In the first part of this work literature-based overview of the problems related to applying LIBS for tokamak diagnostics is given. Second part describes the experimental setup, linear plasma devices, *post-mortem* characterization techniques and the samples used in the experiments. Third part is dedicated to the experimental results. Four journal papers [I]–[IV] are included in this work. From the results described in these papers, in the main part of the thesis only the most important results are given, while unpublished results are described in detail. Author's other related publications are [a]–[e]. In the fourth part results are concluded and the open problems and further perspectives are shortly discussed.

CHAPTER 1: THEORETICAL BACKGROUND

1.1. Laser-induced breakdown spectroscopy (LIBS)

1.1.1. The main idea

In this paragraph the basic principle of LIBS is presented. The description is mainly based on [3]. A pulsed laser beam is focused onto the surface of a substance to be analyzed (Figure 1.1). Radiation energy is locally coupled into the material and the material starts to evaporate. Due to this a crater is formed. The mass of the evaporated material is usually in the range of micrograms. Within this material and the surrounding gas atmosphere (if present) a plasma is generated. The plasma decays and emits element-specific radiation. This emission is resolved spectrally and is detected by a spectrometer. [3]

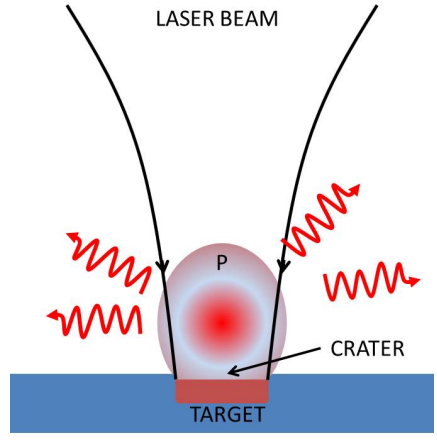

Figure 1.1 Main idea of the LIBS method. Laser beam focused on the target evaporates small part of it and generates plasma (P), a crater is formed.

The life-time of the plasma depends on the laser beam parameters chosen, the conditions of the surrounding gas atmosphere and the substance to be analyzed. Typically, it is in the range of 0.5–10 μs. In vacuum the plasma life-time is usually up to 1 μs. During the life-time of the plasma the emission spectrum changes (Figure 1.2). Shortly after the laser pulse the plasma emits predominately a continuous spectrum, caused by the free-free transitions of electrons (bremsstrahlung) (Figure 1.2a). Only small peaks of the spectral lines of atoms and ions are visible. Afterwards plasma cools down and the intensity of the line emission, as well as the ratio peak intensity to continuous background, increases significantly (Figure 1.2b). In the end of the plasma life-time the temperature decreases further and the emission intensities decrease (Figure 1.2c). Thus, intensity at given wavelength is a function of time $I(\lambda, t)$.[3]

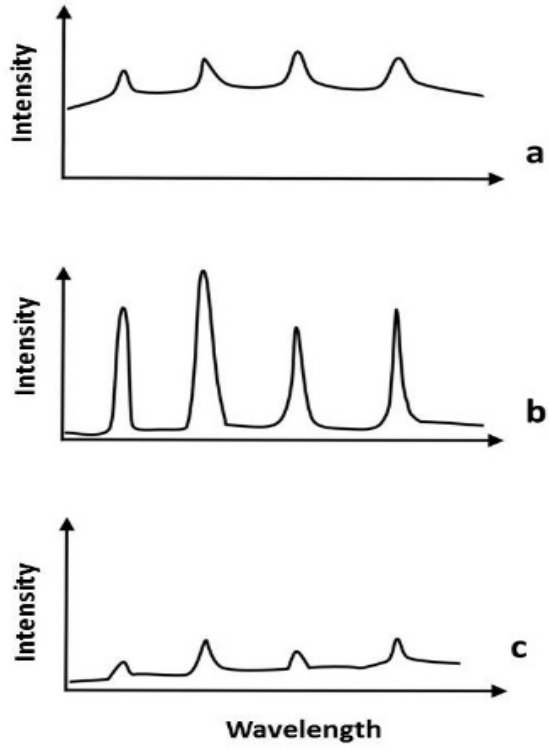

Figure 1.2 Development of a LIBS spectrum as a function of time: a) continuum radiation dominating b) atomic lines dominating c) atomic lines diminishing

1.1.2. Dynamics of the laser-induced plasma

For LIBS of solid samples, the laser radiation evaporates the material and excites spontaneous emission of the material species [4].

LIBS plasma dynamics depends on various parameters, most important are:

1. Laser pulse parameters (wavelength λ, duration τ, energy E, fluence Φ)
2. Target composition
3. Ambient pressure and gas composition

The following description of the plasma plume development is mainly based on [4]. After the laser pulse, the induced plasma will continue to expand into the ambient space. The electron density and temperature of the plasma changes as the plasma expands. Plasma expansion depends on the amount and properties of the ablated mass, the energy coupled into the mass, the spot size of the laser beam, and the environment.

Hot electrons, atomic and ionic mass leave the sample surface. The expansion of the evaporated material into vacuum can be described by the Euler equations of hydrodynamics [5].

In vacuum, the laser induced plasma plume expands adiabatically. The expansion speed can be expressed by

$$v_p = \sqrt{\frac{4\gamma+10}{3}\frac{E}{M_v}} \qquad (1.1)$$

Where v_p is the velocity, γ is the specific heat ratio, E is the energy supporting the expansion and M_v is the total vaporized sample mass within the plume.
When ablation occurs into a gas (or liquid) environment, the ejected mass compresses the surrounding media and produces shockwave. The plasma is a mixture of atoms and ions, and mass from both the ablated target material and the ambient gas. The interaction between the plume and surrounding media slows the expansion of the plasma. The temperature will be higher than that for free expansion. Temperature and number density of ablated mass depend on the properties of the surrounding media.

After the shockwave formation its expansion distance can be described by Sedov's theory [6]. The expansion distance H, can be calculated as function of time:

$$H = \lambda_0 \left(\frac{E_0}{\rho_1}\right)^{1/(2+d)} t^{2/(2+d)} \qquad (1.2)$$

Where the parameter d is the dimensionality of the propagation (for spherical propagation d=3, for cylindrical d=2 and for planar d=1), λ_0 is a dimensionless constant, E_0 energy per area (planar), energy per length (cylindrical) or energy (spherical). The dimensionality of expansion can be determined by fitting the experimental data with equation (H).

Once the plume pressure equalizes to the pressure of the surrounding media the expansion stops. The stopping time is in the range of microseconds. The final distance determines the volume of the plume. LIBS performance depends on the electron density and temperature of the plasma, which strongly depends on the plume volume. [4]

Due to the transient nature of the laser-induced plasma, the following temporal parameters are crucial for LIBS experiments (Figure 1.3):

(a) Delay time (t_d) – the time between the laser pulse and the beginning of the light recording.
(b) Recording time-gate (Δt) – the time interval during that the spectrometer or the camera is recording.

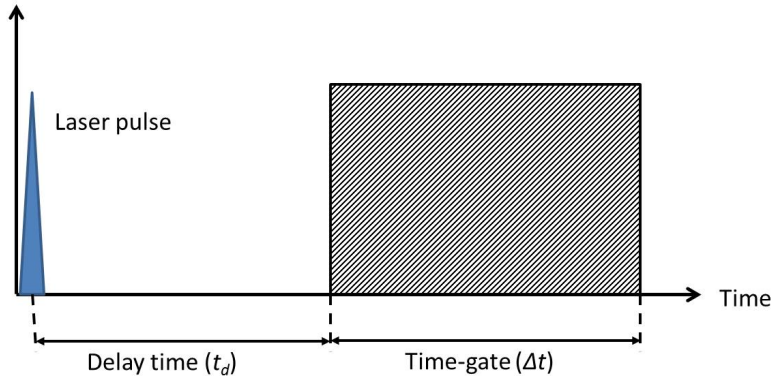

Figure 1.3 Temporal parameters in LIBS experiments

1.1.3. Basic processing of the LIBS spectra

The output of a LIBS measurement is a spectrum where the intensity is represented as a function of the wavelength λ. In most cases relative intensity is measured. In this work the relative intensity calibration is carried out in the means of photon number (counts) not in the energetic units.

From the recorded spectra several measurands are calculated and used as input for the data processing.

(a) Background intensity ($I_B(\lambda)$) is the spectral intensity caused by the continuous background at the given wavelength.

(b) Intensity of a spectral line (I_λ) with the central wavelength λ_c and FWHM $\Delta\lambda$ is calculated as

$$I_\lambda = \int_{\lambda_c-\Delta\lambda}^{\lambda_c+\Delta\lambda} I_c(\lambda)d\lambda. \qquad (1.3)$$

Here I_c is the background corrected intensity that is calculated as

$$I_c(\lambda) = I(\lambda) - I_B(\lambda). \qquad (1.4)$$

In real experiments the wavelength scale is discrete and the integration is replaced by summation.

(c) Total intensity (I_I) is calculated as the integral over the measured spectral range (from λ_{min} to λ_{max}) as

$$I_I = \int_{\lambda_{min}}^{\lambda_{max}} I(\lambda)d\lambda. \qquad (1.5)$$

Both the background intensity and the line intensities are taken into account.

In some cases, it is possible to increase the signal-to-noise ratio (SNR) by fitting the experimental data with analytical curves (usually the emission lines are fitted with Lorentzian, Gaussian or Voigt profiles).

1.1.4. Data processing: elemental depth profiles and averaging

In general case, the samples have elemental composition gradients along the surface and also perpendicular to that. Meanwhile spatially resolved measurements along the surface are done by moving the sample or scanning the laser beam, the measurements of elemental distribution perpendicular to the surface needs more complicated approach [3]. For this purpose elemental depth profiles are calculated by recording the spectrum as a function of the laser shot number. In addition, the ablation rate (thickness of the ablated layer per laser pulse) has to be known. For example, elemental depth profiles are applied to study erosion and deposition effects. In the ideal case elemental depth-profiles describe the relative concentration of the species in the sample as a function of depth. To establish this several methods are applied.

To increase the SNR, averaging algorithms are used. Generally, the sample composition for every laser shot is different and therefore simple averaging is not applicable. In case of multiline averaging [7] a number of spectral lines belonging to selected species are averaged. Weighted average could be applied, giving larger weights to more reliable spectral lines. If the sample composition along its surface is more-or-less homogeneous, multisite averaging [8] could be applied. Spectra from different craters are averaged to increase the SNR. Meanwhile the laser fluence could be kept low, providing good depth resolution. In case of thick coatings “moving average” could be applied [9].

Intensities found from the spectra are converted in most cases to relative concentrations of the species present in the sample. This could be done by calibration curves or calibration free LIBS (CF-LIBS) approach (see 1.1.5–1.1.7). In some cases absolute concentrations of species are estimated [10].

To receive elemental depth profiles the laser shot number is converted to depth. For that the ablation rate has to be known. In the simplest case the ablation rate is assumed to be constant. This is usually true for the bulk samples with small amount of trace elements. In more complicated cases the ablation rate is varying due to the change of the sample composition and structure. To take this into account, the ablation rate has to be calculated as a function of sample composition and properties. These properties have to be known from LIBS or other measurements.

An alternative approach for calculating depth profiles for thick coatings is presented in [11]. This algorithm is based on the statistical correlation of the spectra and needs no prior knowledge of spectral lines etc. Nevertheless, for this approach some calibration points are needed.

An algorithm suitable for calculating depth profiles and decreasing fluctuations in case of thin layers or high ablation is introduced in [II]. This

algorithm does not assume knowledge about the plasma parameters. In addition, the LTE is not assumed. Nevertheless, the concentration proportionality to the line intensity, thus negligible self-absorption is still assumed. Global and local normalization are introduced to reduce the experimental shot-to-shot fluctuations. Due to this the algorithm is suitable for analyzing thin layers where other averaging methods (for example moving average and multisite averaging) are not applicable.

1.1.5. Calibration free LIBS (CF-LIBS): idea and requirements

To gain quantitative results from LIBS there are two main approaches. In case of samples with properties within known limits a prior calibration could be carried out. This is a common practice in metallurgy [3], food analyzing and geology [12]. In some cases this kind of prior calibration is not possible. For these cases CF-LIBS approach could be applied. CF-LIBS is a method to calculate from the LIBS spectra the relative elemental composition of the sample without prior knowledge of the sample composition.

Assumptions made in CF-LIBS approach [13]:

1) The plasma composition is representative of the unperturbed target composition.
2) The plasma is in local thermodynamic equilibrium (LTE) in the temporal and spatial observation window. (see 1.1.7)
3) The plasma can be modeled as a spatially homogeneous source.
4) The spectral lines included in the calculation are optically thin (see 3.1.2).

1.1.6. Boltzmann diagrams

In LTE, excited levels are populated according to the Boltzmann distribution and ionization states are populated according to the Saha-Boltzmann equilibrium equation. The graphical representation of a group of spectral lines in a Boltzmann plane is commonly used to determine the plasma temperature (Boltzmann diagrams). Each spectral line is represented as a point in the plane where the x coordinate corresponds to the energy of the upper level of the transition and the y coordinate to the logarithm of the line intensity divided by the transition probability and degeneracy. The plasma temperature is obtained by linear regression of the points representing lines of the same species, namely by taking the reciprocal of the slope. This is well known approach to determine excitation temperature T_{exc} from the spectral lines intensity. The novelty of CF-LIBS is in the use of the second linear regression parameter, the intercept value, which is a function of the atomic density of the individual species in the plasma:

$$q_s = \log\left(\frac{Fn_s}{U_s(T)}\right) \qquad (1.6)$$

Where the $U_s(T)$ is the value of partition function of the species *s* at the temperature *T* and *F* is unknown parameter which accounts for the absolute efficiency of the detection system. The atomic density of each species can be thus derived by inversion of Equation 1.6. [13]

1.1.7. Local thermodynamic equilibrium (LTE)

The following analyze of the LTE is based on [14]. LTE is a necessary requirement for applying calibration-free LIBS (CF-LIBS) approach (see 1.1.5). In laser-induced plasmas, as well as in most laboratory plasmas, the radiative energy is decoupled from the other forms of energy, since radiative equilibrium requires the plasma to be optically thick at all frequencies (black body). When photons escape from the plasma, their energy distribution deviates from the Planck function and this inevitably affects also the balances involving electrons, atoms and ions. However, if the energy lost by radiation is smaller than that involved in the other processes involving material species, the Saha-Boltzmann and Maxwell distributions are still a valid description of the system and a new equilibrium, LTE, is settled. In case of stationary and homogenous plasma LTE conditions can be tested by following a criterion, which is usually referred to as the McWhirter criterion. In a semi-classical treatment one possible form of the McWhirter criterion is

$$n_e(cm^{-3}) > 1.6 \cdot 10^{12}\sqrt{T}(\Delta E_{nm})^3 \qquad (1.7)$$

where the electron temperature *T* and the spectral transition energy ΔE_{nm} are expressed in K and eV, respectively. n_e is the electron density. In LIBS plasmas the fulfillment of the McWhirter criterion cannot be sufficient for assessing the validity of LTE [14]. Nevertheless, as the fulfillment of this criterion is relatively easy to calculate from the experimental data, in number of works (for example [15], [16], [17]) it is the main test for LTE.

In case of transient plasma in addition to the McWhirter criterion the relaxation time τ_{rel} of the plasma (the time needed for the establishment of excitation and ionization equilibria) is much shorter than the time of variation of thermodynamic parameter. The following relations must hold:

$$\frac{T(t+\tau_{rel})-T(t)}{T(t)} \ll 1 \qquad (1.8)$$

$$\frac{n_e(t+\tau_{rel})-n_e(t)}{n_e(t)} \ll 1 \qquad (1.9)$$

In case of inhomogeneous plasma a third criterion must be satisfied. This criterion requires that the diffusion length of atoms and ions during a time period of the order of the relaxation time to the equilibrium is shorter than the variation

length of temperature and electron number density. This condition at the position x can be expressed as

$$\frac{T(x)-T(x+\lambda)}{T(x)} \ll 1 \qquad (1.10)$$

$$\frac{n_e(x)-n_e(x+\lambda)}{n_e(x)} \ll 1 \qquad (1.11)$$

Here $\lambda = \sqrt{D \cdot \tau_{rel}}$ is the diffusion length during the relaxation time (D is the diffusion coefficient). Detailed description of calculating τ_{rel}, λ and D are given in [14].

In vacuum due to the fast expansion n_e is low, especially for short delay times. Meanwhile the electron temperature T_e is high. Therefore, the fulfillment of LTE is doubtful. [14]

On the other hand, for longer delay times the self-absorption for spectral lines is usually stronger [18], therefore the applicability of CF-LIBS at low pressure is problematic.

1.2. Plasma surface interaction (PSI)

1.2.1. General considerations

PSI has been a critical issue in tokamak design and an important research topic from the introduction of the tokamak concept in 1950s [19], [20]. The properties of plasma facing components (PFC) will affect strongly the lifetime of the reactor elements, tritium (T) inventory, plasma contamination and operation. For a long time, carbon-fiber-compounds (CFC) were considered as a strong candidate to become a material for PFC in ITER. Finally, it was discarded because its behavior under neutron irradiance (Table 1.1). After a long discussion and research of different possibilities including experiments on Joint European Torus (JET) [21], [22] it has been decided that tungsten (W) will be the material for the divertor and beryllium (Be) for the first wall in ITER. The main properties of W, Be and CFC are compared in Table 1.1.

PSI includes various chemical and physical processes like heat loads, erosion, ablation, melting, implantation etc. The largest damage of reactor walls is caused by plasma instabilities – edge localised modes (ELM). In this case the heat load reaches 10 MWm^{-2} order of magnitude [23].

From the viewpoint of safety one of the main concerns in the ITER design is the T retention. There is a limit for the in-vessel mobilizable T inventory in ITER. An allowable safety limit for the T inventory of 1 kg was imposed; the eventual administrative limit (due to the uncertainty in measuring T amount) will be 700 g [24]. To estimate the amount of T and deuterium (D) in the walls an online technique is needed. Due to the radioactivity of T (β-decay, half-life 12.3 years) in this work D containing samples were tested.

Table 1.1. Comparison of W, Be and CFC properties

	W	Be	CFC
Atomic number Z	74	4	6
Maximal allowable concentration	20 ppm	3 %	2 %
Thermal conductivity [W/mK]	140	190	200–500
Melting point [C]	3410	1285	> 2200 (sublimation)
Thermal expansion [10^{-6} K^{-1}]	4.5	11.5	0
Neutron radiation effect	Activation	Swelling	Decrease in thermal conductivity

1.2.2. Results of ITER-relevant materials studies

W is selected for the ITER divertor because of its very high melting point (3695 K) and good thermal conductivity (173 W/(m·K)). Main drawbacks for the W are the mechanical properties (brittleness, cracking) and high Z-number (74). Due to the Z-number W impurities in the plasma cause radiation losses and the maximum acceptable concentration of W particles is very low (approximately 20 ppm). In addition, W has poor mechanical properties: at temperatures below 600 ºC W is brittle and might be not able to withstand thermal shocks etc. Therefore, PSI study on W concentrates on its mechanical properties and erosion under steady-state and pulsed (ELM) regime. [25]

W interaction with D and helium (He) plasma is studied in many works (for example [26], [27]). These works show that even at ion energies clearly below the sputtering threshold, noticeable modifications at W surface are observed. These modifications enhance T, D retention and may decrease thermal conductivity. Also ELM simulations on W samples have been carried out with different methods: laser pulses, electron beam and pulsed plasma sources [28], [29].

Although Be is selected as one of the main materials for ITER first wall [30], the data of Be behavior under ITER-relevant plasma fluxes is limited. Information about Be performing as a material for PFC is gained from JET campaign with ITER-like wall (started in September 2011). These experiments show that in W/Be device most of the long-term fuel retention is caused by co-deposited Be and residual impurities [31]. Experiments on PISCES device show that there are contradictions between the models and experimental results of Be erosion study. The evolution of complicated surface morphology is seen to reduce the erosion 2–3 times [32]. Computer code modeling has been also applied to study Be erosion and redeposition in tokamak [33].

However, the usage of Be in laboratory experiments is limited by its toxicity. In number of cases a proxy is needed for many experiments. Due to the similarity of its electronegativity, Al can successfully resemble Be in terms of formation of compounds especially the oxides and possibly the hydrides. The other candidate magnesium is not suitable in the means of for a possible hydride deposit formation. [34]

1.2.3. LIBS as a method for monitoring PSI processes: results, current problems and limitations

The development of LIBS for characterization of PFC of fusion reactors is under study in numerous scientific laboratories. Many problems, met in application of LIBS at fusion-related studies are characteristic to LIBS in general (problems with SNR for single shot and remote recording, methods of quantitative analysis etc. [35], [36]). At the same time LIBS for fusion and for PSI studies in more general has its peculiarities [37]. The thermal and ablation properties of ITER-relevant materials (Be, W) differ considerably. Due to the plasma action the surface morphology and phase structure of PFC changes which could alter the ablation rate. *In-situ* LIBS for first wall testing assumes the measurements in vacuum. In vacuum the plasma plume expands rapidly and compared with atmospheric pressure background, the charged particle concentrations and plasma temperature are considerably lower.

In addition to the general limitations there are problems related to specific elements. In case of W there is a very limited number of spectral lines which have acceptable values of SNR and small enough self-absorption [e]. In addition to that, numerous weak W lines give a remarkable contribution to the continuum background signal. In this work a study [I] is carried out to select the most suitable W spectral lines for quantitative analyzes.

As mentioned above, in case of Be the biggest problem is the toxicity. Most of LIBS groups tested samples where Al has been used as a proxy for Be. Most consistent LIBS studies with Be-containing tokamak-relevant samples were carried out in VTT, Finland [38], [a]. Elemental depth profiling of samples surface, built on the basis of LIBS measurements, showed a qualitative matching with results obtained by different surface characterization methods. It should be emphasized that from the viewpoint of LIBS Al and Be spectra are remarkably different and for the ITER application and selection of suitable spectral line set, LIBS experiments on Be containing samples are necessary. Nevertheless, recent experiments in VTT [39] have demonstrated that the ablation rate for Be/W and Al/W samples are nearly the same. In the LIBS setup used in current work it is not possible to handle samples containing Be. Therefore, Al as a proxy material of Be is used.

The biggest problems in fuel retention studies are the recording system sensitivity and the separation of H isotopes, the wavelengths for the Balmer α-line for T, D and H are 656.04 nm, 656.10 nm and 656.28 nm, respectively. These lines are strongly influenced by Stark broadening caused by high electron density in LIBS plasma, especially in case of short delay times and high ambient pressure [40]. In addition to that a segregation of H isotopes in laser-induced plasma plume might occur [41]. Plasma parameters and ionization degree play an important role: ions of H isotopes do not radiate line emission. In this work the main effort for this topic is developing methodology for D *in-situ* detection from W samples.

CHAPTER 2: EXPERIMENTAL

2.1. Setup

2.1.1. Domestic LIBS setup

A table-top LIBS setup was used to carry out *post-mortem* LIBS analyzes and studies dedicated to the fundamental aspects of W laser induced plasma. Main parts of the setup are the Nd:YAG laser, the vacuum chamber, and the spectrometers.

Most of the LIBS studies were made using pulsed (FWHM = 8 ns) Nd:YAG laser Quantel YG981C at fundamental wavelength 1064 nm. Besides, the harmonics at 532 nm and 266 nm were used. The maximum pulse energy at 1064 nm is around 1 J, at shorter wavelengths it is 2-4 times lower. The laser beam had the Gaussian shape with 10 mm FWHM. It should be noticed that since the beam profile is not top-hat, it has strong influence to the calculated elemental depth profiles [42].

The vacuum chamber had volume around 25 L and was equipped with turbomolecular and rotary vane pump. The minimal achievable residual pressure was 10^{-6} mbar. The chamber has 5 viewing ports at 0º, 45º and 90º direction to the target normal (Figure 2.1). The chamber is equipped with electric feed-throughs and X-Y moving stage for target mounting. The X-Y stage is moved by stepper-motors controlled by PC.

During the experiments two spectrometers were used. First one was Echelle type spectrometer Andor Mechelle 5000 with Andor iCCD (1024 x 1024 pixels) camera which record spectrum during a single laser shot in 220–850 nm range. The resolution of the spectrometer ($\lambda/\Delta\lambda$) was 5000. For every wavelength 3–5 vertical pixels were pinned. The light was guided to the spectrometer via optical fiber of 50 μm diameter. For the Mechelle 5000 spectrometer the relative intensity calibration was carried out using the Ocean Optics UV-VIS-NIR calibration source DH-2000. The second, Czerny-Turner type spectrometer MDR-23 was coupled with Andor ICCD camera (512 x 2048 pixels). The device recorded the spectra between 300-700 nm in a preselected range of 20 nm width. With 40 μm entrance slit and 1200 lines/mm grating the spectral resolution ($\lambda/\Delta\lambda$) was 6500. For every wavelength 500 pixels were pinned. Two setups were used to guide the light to the entrance slit of MDR-23 spectrometer. With the first setup the light was guided to the spectrometer slit via fiber bundle consisting of fifty 120 μm diameter fibers. The fibers at the spectrometer slit were arranged as linear array (7 mm x 0.1 mm) to enable more efficient light harvesting. The other end of the fiber bundle was circular (0.8 mm in diameter*)*. With the other setup the light was imaged to the entrance slit with a lens.

To guide the light to the end of the optical fiber, different kind of collimating optical systems were used. For the Echelle spectrometer, operating in wide spectral range, off-axis parabola mirrors were preferred, mainly because of lack

of the chromatic aberration. For narrow spectral ranges (20 nm) mainly lenses were used.

The same Andor ICCD camera (512 x 2048 pixels) was applied to record images of the plasma plume. It was equipped with photo-lens (f=250 mm) and different filters.

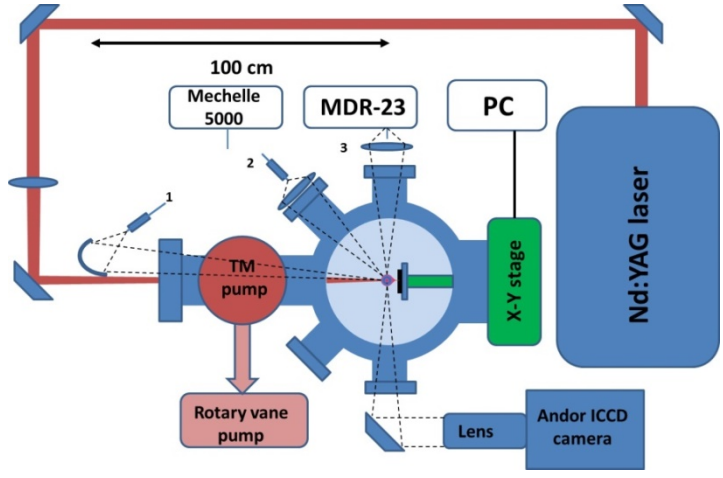

Figure 2.1. Domestic LIBS setup

2.1.2. Linear plasma machines Pilot-PSI and Magnum-PSI

Pilot-PSI (Figure 2.2) and Magnum-PSI (Figure 2.3 [43]) are linear plasma devices in FOM Institute DIFFER (The Netherlands), which are designed for the study of plasma surface interactions under fusion relevant conditions. Pilot-PSI is a forerunner for Magnum-PSI. Nevertheless, due to its smaller dimensions higher particle fluences are achievable in Pilot-PSI in reasonable experimental time.

Cascaded arc plasma sources are used to generate the high density plasma. More specific description is given in [44] and [45]. The plasma jet created in the source is confined and aimed by the strong axial magnetic field (up to 1.6 T in Pilot-PSI) to the tested sample, in this way the source creates high fluxes.

Typical parameters of the plasma beam for the devices: electron density (n_e) 10^{19}–10^{21} m^{-3}, electron temperature (T_e) 0.1–10 eV, particle flux 10^{23}–10^{25} m^{-2} s^{-1}. The energy of ions is controlled by the bias voltage of the target.

Specific plasma regimes used in the experiments are described in the corresponding chapters.

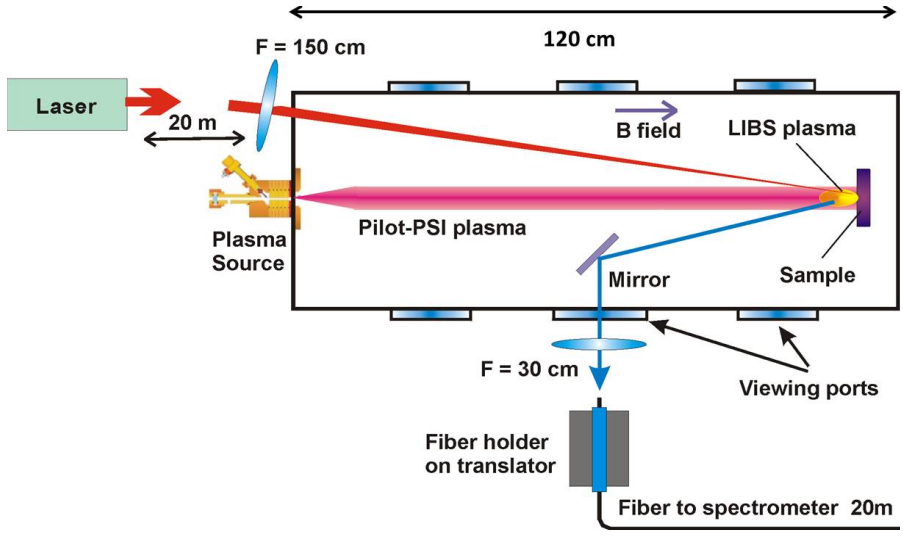

Figure 2.2. Pilot-PSI with LIBS setup

In most cases the particle distribution in the plasma beam is Gaussian (FWHM 12–25 mm). Nevertheless, due to the effects caused by the $\vec{E} \times \vec{B}$ rotation [46], molecular recombination, and effects of the plasma sheath at the target surface [47] different distributions are observed, especially in cases of plasmas that consist of different species. By biasing the target, the electron and ion bombardment ratio could be controlled at various regions on the target [48].

In addition to the vacuum vessel size in Magnum-PSI one of the biggest enhancements compared to the Pilot-PSI is the target mounting system. This system consists of the user-defined target head, the target manipulator and the target exchange chamber. The target manipulator allows moving the target to the target exchange and analyzes chamber (TEAC). The manipulator can be rotated by ±120° and allows tilting of the target against the magnetic field in a range of ±90° (with 0° being perpendicular to the magnetic field) [49]. In the future Magnum-PSI is planned to operate with a superconductive magnet.

The plasma conditions (n_e and T_e) are monitored with Thomson scattering [50] at various positions respect to the target. Interactions between the plasma and the target are monitored with emission spectroscopy, IR-thermography, spectral pyrometer and fast visible light camera.

In previous studies samples exposed to Pilot-PSI plasma have been tested with *post-mortem* LIBS in a device similar to the setup described in 2.1.1 [51]. In the framework of the current study also an *in-situ* LIBS system was installed for both Pilot-PSI and Magnum-PSI.

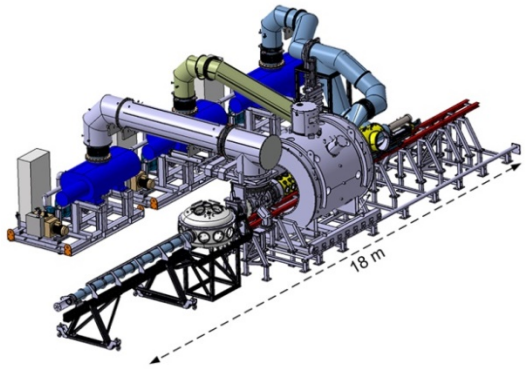

Figure 2.3 Magnum-PSI device [43]

LIBS measurements in Magnum-PSI were carried out in the target exchange and analyzes chamber (TEAC). Spatial scanning was achieved by using the manipulator described above. The detailed description of the LIBS setup used in Magnum-PSI is in [II] and also in [b].

Figure 2.2 gives also a sketch of LIBS setup used for *in-situ* measurements in Pilot-PSI. Actually, the plane determined by the Pilot-PSI plasma and laser beam was vertical, while the details of the recording part were aligned in the horizontal plane.

Nd:YAG laser lasing at 1064 nm, with pulse duration 8 ns was applied for the LIBS measurements. The laser was at approximately 20 m distance from the Pilot-PSI device. The laser beam was first expanded to the diameter of 3 cm and then it was guided via mirrors to the device where lenses of 1.5 m effective focus lens focused the beam to the sample. Laser pulse energy at the sample surface was 160 mJ and the area of the laser spot was approximately 1 mm^2 corresponding to the fluence 16 J/cm^2. Using a plane mirror and a lens of 30 cm focal length, the radiation of the laser-produced plasma was directed to the end of a fiber of 0.8 mm diameter, which delivered the radiation to the spectrometer location. Length of the fiber was approximately 20 m. Magnification of the plasma image at the fiber end was close to unity. The other end of the fiber was coupled to a fiber bundle consisting of 50 fibers 120 μm in diameter. At the spectrometer entrance the fibers in the bundle were arranged in a linear array. This array was used as an entrance slit. Czerny-Turner spectrometer with 1 meter focal length was coupled with Manta G-145 CCD camera and image intensifier. To the signal at a certain wavelength corresponded the sum of a number of vertically binned ICCD pixels.

Two different gratings were used: 300 lines/mm grating for recording spectra in 420–490 nm spectral range which contained mainly W and Mo lines and 1200 lines/mm line grating for higher resolution measurements of Balmer α-lines of hydrogen isotopes. Delay time t_d was 100 ns for the W and Mo spectra and 200 ns for D/H spectra. In both cases, time-gate Δt was 3 μs.

Spectra containing W and Mo lines were recorded at the Pilot-PSI background pressure 10^{-3} mbar while lines of hydrogen isotopes were reliably recorded in Ar at 1.2 mbar pressure.

LIBS measurements were carried out *in-situ* conditions right after the plasma exposure. Spectra as a function of the number of laser shots were recorded from a number of different spots corresponding to the areas on the sample with different surface modifications caused by Pilot-PSI plasma.

2.1.3. Additional surface characterization methods

Scanning electron microscopy (SEM)

SEM was the main method for describing the structures at the surface of the samples. The Helios™ NanoLab 600 (FEI) SEM device was applied to characterize the surface morphology and structure. Magnifications from 1000 to 80 000 were applied. The applied voltage was 2 kV. Measurements were carried out at Institute of Physics, University of Tartu, Estonia.

X-ray diffraction (XRD)

XRD measurements were carried out using SmartLab (Rigaku) diffractometer. The wavelength of the X-ray radiation was 1.54 Å (Cu Kα line). The XRD spectra were measured from 30 to 80 degrees. Radiation was generated with 45 kV high voltage and 180 mA current. Measurements were carried out at Institute of Physics, University of Tartu, Estonia.

Secondary ion mass spectroscopy (SIMS)

Quadropole mass spectrometer VG Ionex IX-70S with O_2^+ primary ion beam was applied. Measurements were carried out at VTT, Finland.

Particle-induced X-ray emission ion micro beam (μ-beam) analyzes

Particle-induced X-ray emission (PIXE) measurements with micro-beam were performed using the 2-MV tandem accelerator were carried out on micro-beam beam line, which is located at -10° from the exit of the accelerator. Micro-beam experimental line coupled with high brightness multicusp ion source, with proton beam which can be focused to dimensions of 500X500 nm^2. Measurements were carried out at the Jožef Stefan Institute, Slovenia.

Nuclear reaction analyzes (NRA)

For NRA measurements ^{3}He beam was used, ^{3}He+ ions were created in duoplasmatron ion source. The duoplasmatron ion source is permanently configured for production of He ion beam. To optimize the consumption of ^{3}He gas a mixing apparatus was constructed for mixing ^{3}He and ^{4}He gasses. An analytical current of 300 pA was used. ^{3}He beam at the energy of 3.3 MeV was focused to 10X10 μm^2. Measurements were carried out at the Jožef Stefan Institute, Slovenia.

2.2. Samples

Three kind of coated samples were used in the studies. In addition to that, measurements on a bulk W sample were carried out.

Samples used for plasma exposure experiments on Pilot-PSI and Magnum-PSI were produced in the DIARC company (Finland). 1.5–2 μm thick coatings were produced on 2.5 mm thick 30 mm diameter Mo substrate. Samples were prepared using vacuum arc. The method is described in more detail in [52]. These samples are referred as "DIARC samples" or just "DIARC" in this study. List of the sample types used in the experiments is in the Table 2.1. Most of the samples had pure W coatings. Some samples had Al content from 10 to 40 atomic %. As described in 1.2 Al was used as a proxy for Be that will be used in the ITER. To develop methods for D detection samples with a few atomic percent D doping were also tested.

Two samples had yttrium (Y) doping (up to 5 at. %). Y was used to study its effect on the sputtering yield of W coatings. Previous studies demonstrate that Y content around 1 weight % improves the shock resistance of W [53].

Table 2.1. List of DIARC samples used in the study

Ref. number	Nominal coating thickness (μm)	W (at %)	Al (at %)	Y doping	D doping
1	2/1.5	100	0	-	-
2	2	100	0	-	+
3	2	60	40	-	-
4	2	90	10	-	-
5	2	100	0	+	-
6	2	80	20	-	-
7	2	80	20	-	+

For the study of ablation rate dependence on the surface morphology samples were produced using the magnetron sputtering (MS) [54] method, produced in IAP (Romania). These samples are referred as "IAP samples" or just "IAP" in this study.

To study the applicability of LIBS for analyzing deposited layers and D detection from samples from real tokamaks, samples drilled from ASDEX Upgrade (AUG) tokamak tiles: inner divertor (tile 4) outer divertor (tiles 1 and 3B-II) were used. Positions of the tiles in the tokamak and the samples on the tiles is given in [IV Figure 1]. The tiles were used during the AUG 2009 year campaign with D plasmas. Diameter of the samples was 17 mm. Originally all these samples were 1–10 μm thick tungsten coatings on fine-grained graphite. These samples are referred as "AUG samples" or just "AUG" in this study.

Table 2.2. List of the IAP samples used in the study

Ref. number	Nominal coating thickness (μm)	W (at %)	Al (at %)	Surface	D doping
1	2	100	0	smooth	-
2	2	100	0	rough	-
3	2	100	0	smooth	+
4	2	90	10	smooth	-
5	2	90	10	smooth	+

Table 2.3. List of the AUG samples used in the study

Ref. number	AUG tile	Tile position	Marking
1	1	Outer divertor	1-1
2	1	Outer divertor	1-2
3	4	Inner divertor	4-1b
4	4	Inner divertor	4-2b
5	3B-II	Outer divertor	3B-II-1b
6	3B-II	Outer divertor	3B-II-2b

CHAPTER 3: RESULTS AND DISCUSSION

3.1. Characterization of ITER-relevant materials by time resolved LIBS

3.1.1. Ablation regularities at low (10^{-3} mbar) pressure and 1–2 mbar Ar background pressure

The aim of these experiments was to record temporal and spatial characteristics of the plasma. This information is necessary to find optimal delay times, recording time-gate widths and setup for the plasma plume imaging for the LIBS experiments.

Time-gated images of the plasma plume were recorded with the ICCD camera described in 2.1.1. During the experiments the integral spectral radiation was recorded. Taking into account the spectral sensitivity of the camera and the optical transmission of the photo-lens, the imaging spectral range was 350–800 nm. The delay time t_d ranged from 20 to 300 ns, the recording time-gate Δt was 20 ns.

Measurements were carried out and the ablation properties were studied at 10^{-3} and 1–2 mbar of Ar background pressure, as these conditions were used for D detection in the further experiments.

According to Figure 3.1, at low pressure the plasma plume had a diffuse structure, its linear dimension in the direction of the target normal increased from 1 mm at 50 ns till 3 mm at 350 ns. The maximum intensity at t_d = 300 ns was 2.5 times lower than that was at t_d = 100 ns.

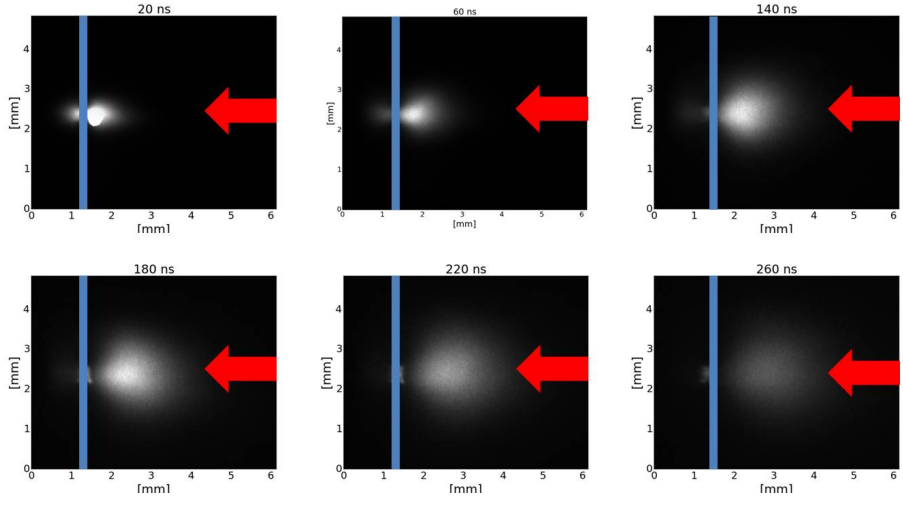

Figure 3.1. Plasma plume development at low pressure. The blue line and the red arrow indicate the target plane and the laser beam direction, respectively. Recording time-gate Δt=20 ns, laser energy E= 60 mJ and wavelength λ= 266 nm. Numbers above the images indicate the delay time t_d.

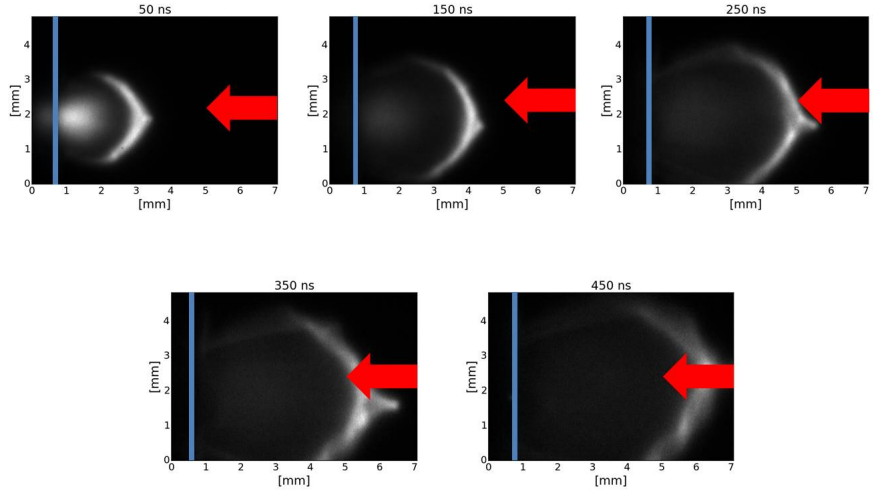

Figure 3.2 Plasma plume development at 1.8 mbar Ar background pressure. The blue line and the red arrow indicate the target plane and the laser beam direction, respectively. Recording time-gate Δt=20 ns, laser energy E= 60 mJ and wavelength λ= 266 nm. Numbers above the images indicate the delay time t_d.

Figure 3.3 describes the plasma expansion (plume position versus time). In case of 10^{-3} mbar the position for the emission maximum of the plasma plume is plotted, in case of 1.8 mbar the position of the luminous front. Data points were fitted with quadratic function to have a differentiable smooth line for the velocity calculation. In Figure 3.4 the plasma plume velocity calculated from the quadratic fit for the position is plotted. At t_d = 100 ns the expansion velocity in vacuum was $1.6 \cdot 10^4$ m/s, at 300 ns it had decreased to $1 \cdot 10^4$ m/s.

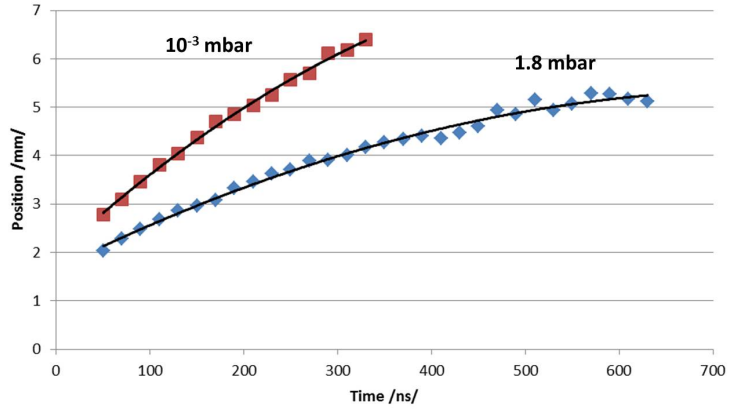

Figure 3.3. Plasma spatial development. Position of the maximum at low pressure (10^{-3} mbar) and position of the front for 1.8 mbar. Data points are fitted with quadratic functions.

At 1.8 mbar pressure the plasma plume structure was different from that in vacuum (Figure 3.2). There was distinct luminous front moving in the background gas. Behind the front there is plasma core which behaves like the plasma plume in the vacuum: its development is diffuse. Similar regularities for the plasma plume expansion have been reported in [55]. At 350 ns delay time the plasma front had reached approximately 4.5 mm from the target. The radiation decay time was noticeably longer: the radiation was observable for several microseconds.

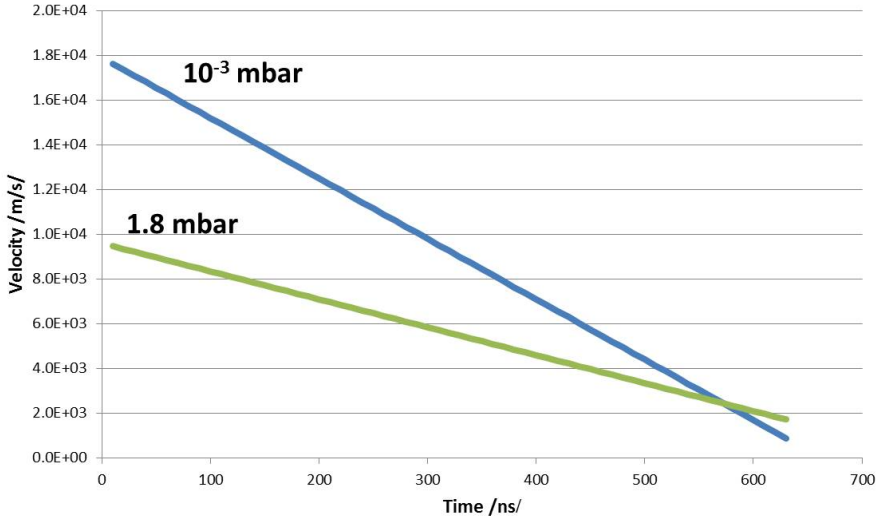

Figure 3.4. Velocity of the plasma plume (calculated according to the quadratic estimation of the plume position).

At 1.8 mbar pressure the expansion velocity was lower: $1 \cdot 10^4$ m/s at 100 ns and $7 \cdot 10^3$ m/s at 300 ns.

The critical pressure in the LIBS experiments was about 10^{-1} mbar above which the plume radiation intensity increased strongly, indicating that the collisions between the plasma particles (neutral atoms and ions) and surrounding gas atoms become important. This argument is supported by the fact that mean free path length at this pressure in the Ar is 2 mm which is comparable to linear dimension of the plasma plume.

3.1.2. Selection of W spectral lines

As a high-Z element, W has a great number of spectral lines. Aim of this study was to find amongst these the most suitable lines for quantitative analyzes. Suitable lines should have high SNR and negligible self-absorption.

Studies carried out at atmospheric pressure [56] have shown that the electron temperature T_e and density n_e of the LIBS plasma depend strongly on the laser wavelength. Our aim was to carry out similar experiments in vacuum and compare the laser wavelengths 266 nm and 1064 nm.

Bulk samples were used to analyze W spectral lines. Details of the study are presented in [I].

In this study the laser wavelengths 1064 and 266 nm were used. The electron temperature of the plasma was calculated on the bases of Boltzmann plots built both for W neutral atoms and ions. Theoretical background of this method is described in 1.1.3. Simple qualitative criteria for estimating the presence of the self-absorption were found. In general, our study demonstrated that the strongest W I spectral lines (400.88, 407.44 and 429.46 nm) with high transition probability and relatively low lower energy state are noticeably self-absorbed. W II lines do not show effects of strong self-absorption. To study the SNR, the relative standard deviation [57] was calculated for the selected spectral region.

Electron temperature was 1.25 eV and 0.6 eV [I Figure 5] at the delay times 100 ns and 500 ns, respectively. There was no clear dependence on the laser wavelength; within the experimental uncertainty the temperatures were identical. For comparison, works carried out at atmospheric pressure have demonstrated that electron temperature and density have clear dependence on the laser wavelength [56].

As a result of the study a set of suitable spectral lines was selected. At the experimental conditions used in the study the electron temperature dependence on the laser wavelength was not observable. Nevertheless, the SNR for the studied spectral lines was in most cases somewhat larger for the laser wavelength 266 nm.

3.1.3. Tests on virgin W coatings

Experiments were carried out to characterize the ablation properties of samples prepared by different methods. LIBS profiles were recorded at a fixed value of fluence. DIARC (Table 2.1, samples 2, 3, 4) and IAP samples (Table 2.2 samples 1, 2, 4) were tested. Results are presented in [58] and [59].

The spectra were recorded with two different spectrometers from different directions: Mechelle 5000 spectrometer looking at 45º to the target normal (Figure 2.2, position 2); MDR-23 looking with the entrance slit at 90º to the target normal (Figure 2.2, position 3).

SEM images of the samples are in the Figure 3.5. Pictures show that compared with the fine structure of DIARC sample, the “smooth” IAP sample has remarkably larger structural elements. Even larger structures are present on the rough IAP samples.

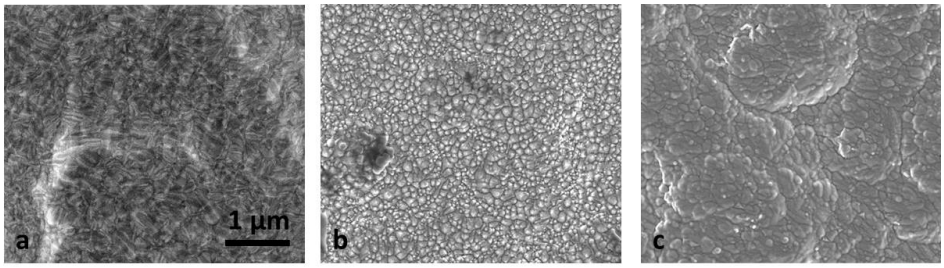

Figure 3.5. SEM images of the tested samples. a) DIARC b) IAP, smooth c) IAP, rough.

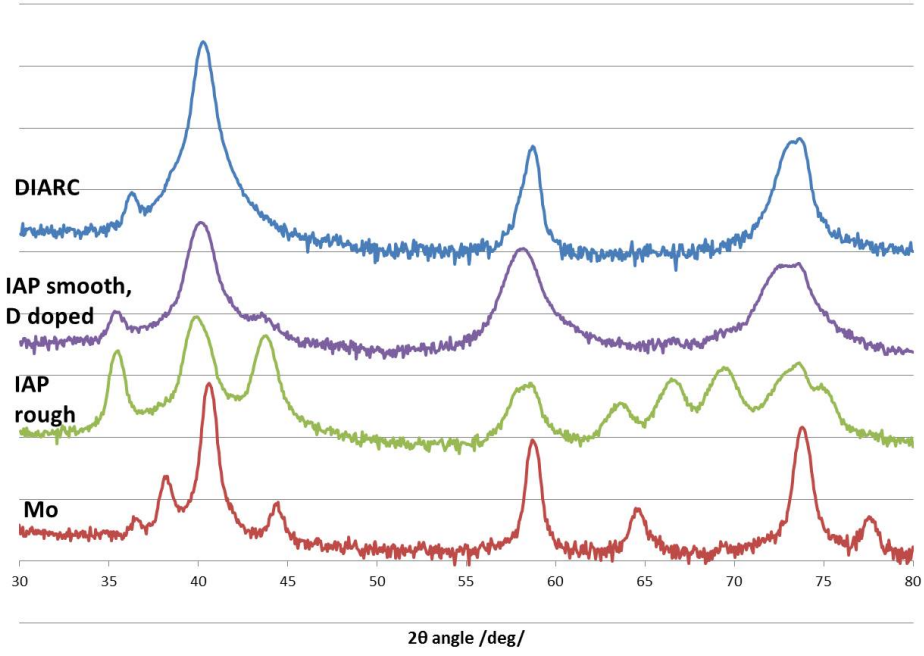

Figure 3.6. XRD spectra of the tested samples and bulk Mo. Intensity is in *log* scale and the baselines are shifted for clarity(originally the background levels are approximately equal).

Recorded XRD spectra (Figure 3.6) show that DIARC samples have narrower lines than smooth IAP samples. That refers to larger crystallites in DIARC coatings. Nevertheless, results may be affected by Mo lines from the substrate. Mo lines are situated near the W lines and may cause apparent line broadening. Rough IAP samples have additional diffraction lines in the range 60–70º, these lines are not present in other spectra. According to the literature [60] these lines

belong to the W metastable β-phase (other lines belong to more common α-phase).

Domestic LIBS setup described in 2.1 was used to carry out the LIBS spectra recording and depth profiling. The laser lased at 532 nm. The laser energy at the sample surface was 80–90 mJ and spot diameter was 0.7 mm, the corresponding average fluence Φ was 7 J/cm^2.

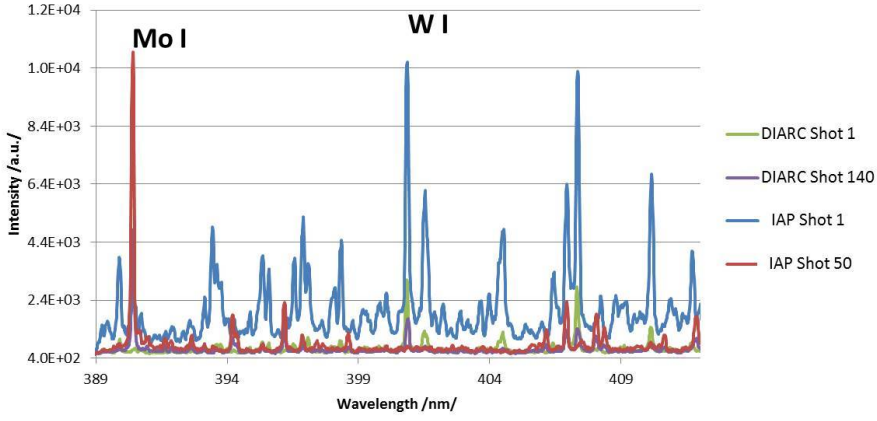

Figure 3.7. Comparison of the measured spectra of the DIARC and IAP samples.

The LIBS spectra in 385–415 nm range were recorded by MDR-23 spectrometer. Examples of the measured spectra are in the Figure 3.7. To build elemental depth profiles strong spectral lines at 390.2 nm (Mo I) and 400.9 nm (W I) were used. Comparison of the elemental depth profiles for the DIARC samples is in the Figure 3.8. To reduce the effect of shot-to-shot fluctuations, trendlines of "moving average" were used. The depth profile for W is not steep and within the measurement uncertainty these profiles for different samples are comparable. This is likely to the crater effects related to the laser beam shape [42], flaking of the coatings etc. The first laser shots recorded at specific site lack of Mo signal, indicating that the laser crater is fully in the W coating. That plateau was used to calculate the ablation rate for the coatings. For pure W coating the plateau is around 29 laser shots, corresponding to ablation rate 69 nm/shot. For the samples containing 10 and 40% Al the ablation rates are 74 nm/shot and 285 nm/shot, respectively. We can see that high Al content increases drastically the ablation rate for the coatings.

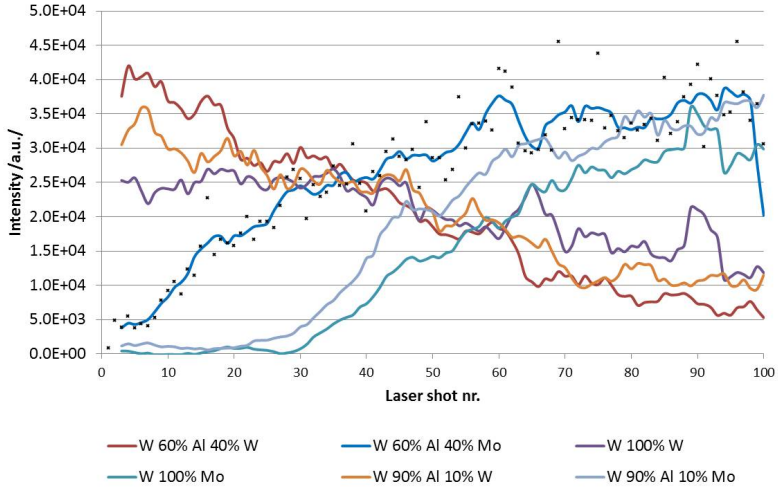

Figure 3.8. Elemental depth profiles (W and Mo) for the DIARC samples. Lines are smoothed using the "moving average". The experimental points in the graph are presented for the sample with 40% Al .

Results of experiments on the IAP samples are in the Figure 3.9. It should be noticed that the x-axis has different scale than in previous graphs for DIARC samples. For pure W coatings a Mo signal well above the noise level is detectable already from the second laser shot. Controversially, for the Al containing samples Mo signal came clearly detectable during the 3–4th laser shot. The continuous background radiation was remarkably stronger during ablating the coating, compared to the continuous background signal obtained from the Mo substrate. That likely indicates enhanced laser radiation absorption and thus more porous structure of the coatings. This is also supported by the SEM images. Due to the small number of laser shots needed to go through the coating, the uncertainty for the ablation rate is high; the ablation rate is roughly in the range of 500 nm/laser shot.

In addition to the intensity of W and Mo spectral lines the total intensity in the measured spectral range was calculated. Figure 3.10 shows that for the DIARC samples (except the one with 40% Al content) this value is nearly independent of the laser shot number. For IAP samples the radiation of the laser-induced plasma generated from the coating is much more intense compared to the one generated from the substrate. This effect could be explained by the enhanced absorption of the laser radiation and smaller thermal conductivity of the IAP coatings.

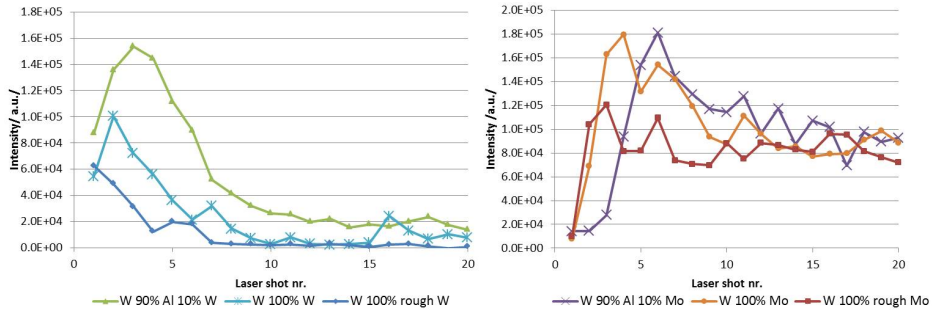

Figure 3.9. Elemental depth profiles of W (left) and Mo (right) for the IAP samples.

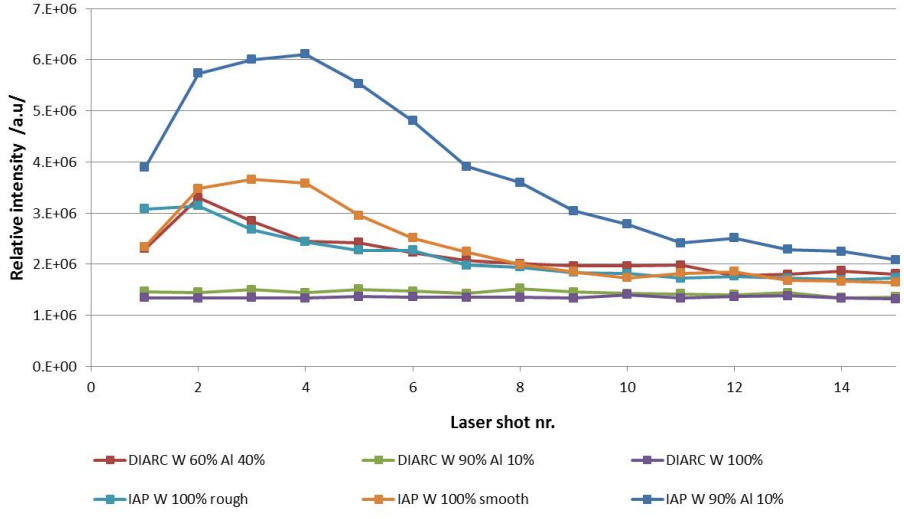

Figure 3.10. Total intensity in the selected spectral region.

Experiments on W coatings with different surface morphology and structure (caused by the production methods) revealed that these parameters have very strong effect on the ablation rate and also on the measured LIBS spectra.

To apply LIBS for *in-situ* erosion and deposition measurements methodology for taking into account the change in the ablation rate should be developed. One possible approach that should be investigated is to use the total intensity or background intensity as a normalization parameter.

3.1.4. D detection from W and W/Al mixture coated samples

Samples with D-doping of 20%Al/80%W coatings were tested (Table 2.1, samples 7). For a comparison samples without D-doping were tested (Table 2.1, samples 6). The results are available in [61].

The experiments were carried out in domestic LIBS device. Laser radiation of λ=1064 nm wavelength was used for excitation of the LIBS spectra. Spectra were recorded at background pressure 10^{-6} mbar setting t_d and Δt to 100 ns and 1000 ns, respectively. Mechelle 5000 spectrometer looking at 0º to the target normal (Figure 2.2, position 1); MDR-23 equipped with the fibre bundle looking at 45º to the target normal (Figure 2.2, position 2). Spectra near the Balmer D_α and H_α lines were recorded with the MDR-23 and in the wide spectral range with Mechelle 5000. The laser fluence Φ was varied from 7 to 10 J/cm^2.

As a preparation for the low pressure measurements also experiments at 1 mbar Ar background pressure were carried out to adjust the experimental setup. These results are not considered here.

Multisite averaging was applied (spectra from 10 sites were averaged). The effect of the averaging is shown in Figure 3.11 left. Figure 3.11 right demonstrates how D_α and H_α lines near 656 nm change with the laser shot number. Clear D peak is detectable only during the second and the third laser shot.

Best results were achieved at a lower fluence value. At higher fluence values the FWHM for D_α and H_α lines was greater mainly due to the Stark broadening [40]. Therefore the spectral lines were not clearly resolved from each other. As the recorded signal was weaker for lower fluence the multisite averaging became important.

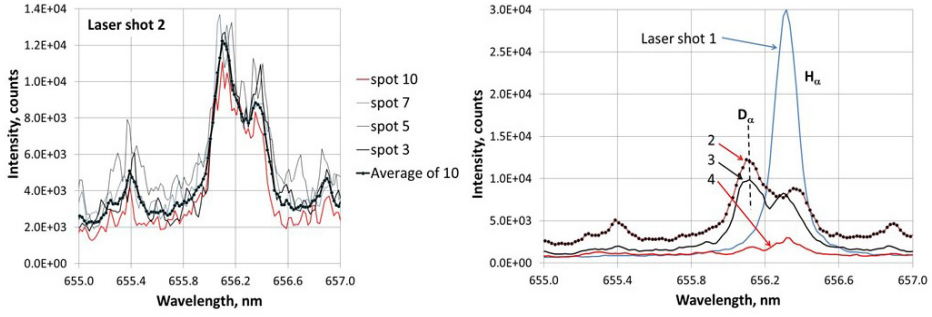

Figure 3.11. Left – multispot averaged spectrum versus single-spot spectra; right – spectrum around 656 nm wavelength as a function of laser shot number.

Figure 3.12 compares the elemental depth profiles of D to the ones of W, Al and Mo. The maxima are normalized to unity. It shows that while D signal is present for three laser shots, the signal for the metals in the coatings persists noticeably longer. Main reason for this phenomenon is expected to be the outgassing of D: first laser shots heat up the sample nearby and the deuterium deeper in the coating is released. Also the difference in recording geometry for D and W/Al might play a role. As shown above (see 3.1.2 and [I]) and known

from the literature [18] self-absorption often affects the line intensity for W and Al lines and thus may disturb the shape of the elemental depth profiles. At high concentrations the intensity of the lines start to saturate and thus the concentration and intensity are not proportional anymore. At low concentration of W or Al gives ill-proportioned high signal that causes "tails" of the elemental depth profiles.

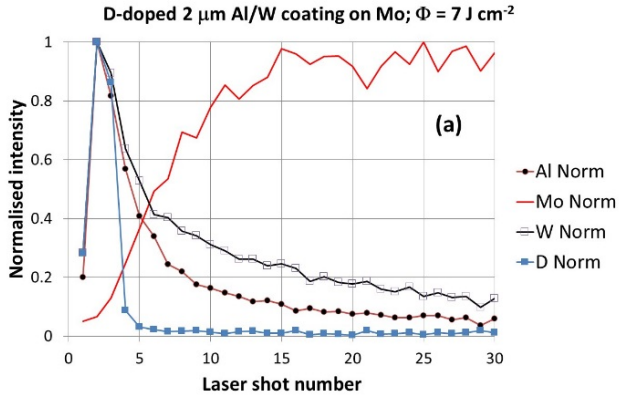

Figure 3.12. Elemental depth profiles for D, W, Mo, Al and Mo (maxima normalized to unity).

With this experiment we showed that it is possible to use LIBS at low background pressure (10^{-6} mbar) to detect Balmer D_α -line and resolve it from the H_α -line. Nevertheless, recording parameters (delay time, time-gate, laser fluence) must be carefully chosen. SNR is also a critical issue for detecting D_α -line and resolving it from the H_α -line.

3.2. Experiments on samples exposed to plasma

3.2.1. Experiments on W coatings exposed to Pilot-PSI He and D plasma

2 μm thick W coatings (Table 2.1 samples 1 and 2 in) were exposed to He and D plasma mixtures in the Pilot-PSI device described in 2.1.2. The composition of the Pilot-PSI plasma, sample surface temperature and ion energy were varied. Sample surface was characterized by SEM. XRD measurements were performed to study the crystal structure. These results are presented in [III].

The SEM images [III Figure 2] demonstrate that the surface structure of W coatings exposed to plasma is strongly dependent on the plasma composition. He containing plasma causes the growth of fuzz-like structure, described in several studies (for example [26], [62]), whereas the changes in the crystal

structure (lattice parameter and crystallite size) were mainly driven by the surface temperature.

Plasma caused erosion of the W coatings and D retention was determined by SIMS and LIBS elemental depth profiles. LIBS measurements were performed with the domestic device described in 2.1. Short overview of the results is published in [d]. The laser fluence during the measurements was approximately 12 J/cm^2. Spectra were recorded with Mechelle 5000 spectrometer in the wide spectral range from 280 nm to 850 nm in collinear direction (Figure 2.1, position 1). In this region a large number of W and Mo atomic lines were distinguishable. Nevertheless, for most of the lines the SNR was low. The applicability of multisite averaging was limited because of the small area of the characteristic regions on exposed samples. It was possible to average spectra only from 2–3 laser craters. With this procedure, acceptable SNR was achieved only for the strongest W spectral lines. The 400.88 nm W I line was used to build the elemental depth profiles. Thus, self-absorption effects are possible. For comparison elemental depth profiles were recorded with LIBS from unexposed samples.

The recorded LIBS spectra show strong dependence on the sample surface morphology. In Figure 3.13 spectra for the two first laser shots are shown for the fuzz-like structure created by He plasma flux and for the unexposed sample. For the fuzz-like structure both the continuum radiation and line emission are much more intense. Continuum is approximately 5 times more intense and the line emission approximately 2.5 times. It could be assumed that in the case of more intense spectra more energy from the laser pulse is coupled to the plasma plume. One straightforward reason for that is following: fuzz-like structure reduces the laser light reflection and increases absorption (at visual observation it looks black, absorption coefficient up to 98% is referred [62]). The increase in the spectra intensity was also present for other surface modifications but it was smaller.

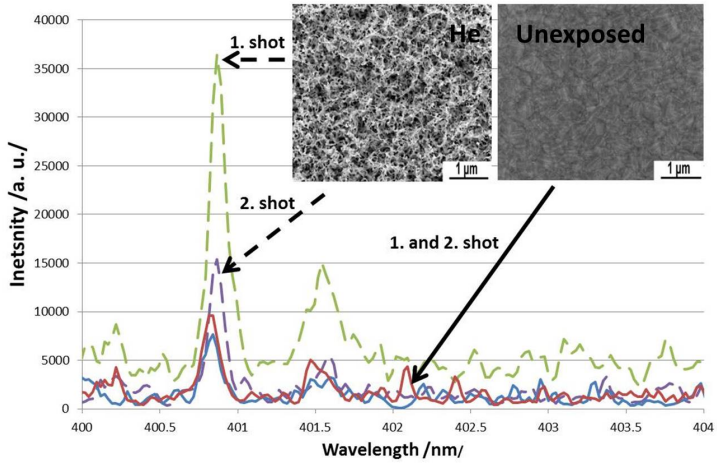

Figure 3.13. Effect of the surface morphology to the recorded LIBS spectra.

The described increase in the intensity is reflected in the W elemental depth profiles (Figure 3.14 left). To overcome this effect a normalization method was introduced: the spectrum was normalized with its total intensity. Figure 3.14 right shows that after the depth profiles become comparable.

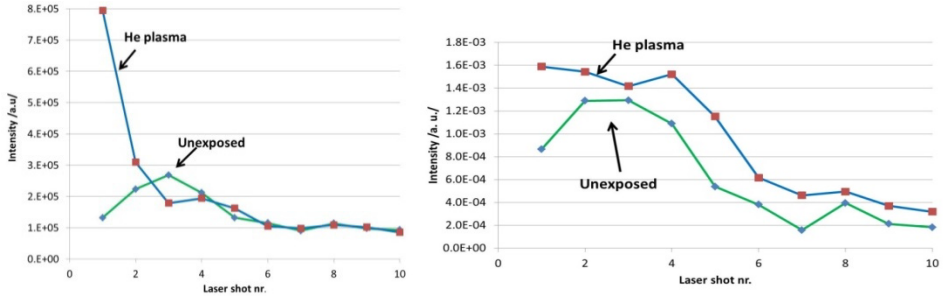

Figure 3.14. Elemental depth profiles for W before (left) and after (right) normalization with the total intensity.

In some regions of the samples exposed to the plasma, Mo spectral lines are observed for a few first laser shots. As SIMS measurements show relatively small erosion of the W coatings, the Mo likely originates from the Mo electrode of Pilot-PSI plasma source or from the clamping ring made of Mo. SIMS measurements also confirm the deposited Mo on the surface. Calculated elemental depth profiles show that it takes 5–6 laser shots to ablate the 2 μm thick W coatings. Thus the ablation rate is 300–400 nm per laser pulse. This result is somewhat controversial with the later study [II] where the laser fluence was comparable (15 J/cm^2) but the ablation rate was assumed to be remarkably lower (200 nm or less). Reason for that is not clear, possible explanations are differences in the used samples (nevertheless, nominal parameters are same for both sample sets used in the experiment) or in the laser beam shape [35] (regions of higher and lower fluence exist in the laser spot; the value given above is a spatial average). Due to the high ablation rate no changes in the coating thickness were distinguishable in the LIBS elemental depth profiles: according to the SIMS measurements the changes in the W coating thickness were less than 100 nm for all the regions of the tested samples.

In this study the effect of surface morphology changes caused by the He and D plasma to the LIBS spectra were studied. It was demonstrated that the morphology has a great influence on the spectra and on the elemental depth profiles recorded by LIBS. The normalization was needed for comparison of the recorded depth profiles. In the further research lower laser fluence has to be used to decrease the ablation rate and thus improve depth resolution for the elemental depth profiles. To make it possible a spectral system with better sensitivity has to be used.

3.2.2. Tests on samples exposed to linear plasma devices and AUG plasma

Samples described in Table 2.3 from the ASDEX Upgrade tokamak were tested in domestic LIBS setup. Experiments were carried out at 1 mbar Ar background pressure. Most detailed analysis was carried out for sample 2b (tile 4) from the inner divertor. This sample had originally W coating on graphite. To increase the SNR multisite averaging was applied. Experimental procedure is described in [IV]. 43 lines of 9 chemical elements were identified from the spectra. Most of them had similar depth profiles [IV Figure 4].

The MDR-23 spectrometer was used to separate D_α and H_α Balmer lines near 656 nm [IV Figure 5]. The H signal is strongest for the first laser shot due to the surface contamination with water vapor. Comparing LIBS data with nuclear reaction analyzes (NRA) it yields that the lowest D concentration detected with LIBS in these experiments was 10^{17} at/cm^2.

We showed that the used LIBS setup allowed reliable detection of D from the AUG tiles. The elemental depth profiles calculated using data processing method described in [II] show reasonable correspondence with relative concentrations obtained by ion-beam methods (SIMS, RBS) [IV Figure 7].

3.3. *In-situ* LIBS measurements on linear plasma devices

3.3.1. *In-situ* LIBS system development on Magnum-PSI

An *in-situ* LIBS setup was applied to measure the erosion of W coatings exposed to Magnum-PSI ELM-like regime. This regime was achieved by adding spikes with 10 Hz repetition rate and 1 ms duration to the Magnum-PSI source current [63]. LIBS measurements were carried out in Magnum-PSI target exchange and analyzes chamber (TEAC). Detailed description of the experiment is in [II].

In this study *in-situ* and *post-mortem* LIBS results were compared [II Figure 5]. Taking into account the difference in laser fluence, good coincidence of the elemental depth profiles was achieved.

It was demonstrated that LIBS is applicable for erosion and deposition measurements in tokamak-like environment. LIBS deduced results were related to the sample surface morphology [II Figure 3].

In addition to that we showed that W coatings used in this study were able to withstand both the steady-state and ELM-like plasma regime used in Magnum-PSI (small ELMs with high repetition rate). The changes in the surface morphology and crystallinity were mainly controlled by the particle fluence and the surface temperature of the sample, the influence of ELMs was small.

3.3.2. *In-situ* LIBS measurements on Pilot-PSI

Samples with 2 μm thick W coatings with and without Y doping (Table 2.1 samples 1 and 5) were tested.

Samples were exposed to D or to D/Ne plasma. Ne component was used to simulate the effect of heavy particles to the processes of plasma-surface interaction: according to [64], at low electron temperature the sputtering yield for Ne ions is comparable to that of W ions. Ne ions should produce cracks and other similar imperfections at the surface, thus enhancing the D retention.

During experiments the plasma's electron density n_e and temperature T_e were $1.4 \cdot 10^{20}$–$3.7 \cdot 10^{20}$ m^{-3} and 1–2 eV, respectively. Four samples were exposed to plasma fluxes. Main characteristics of the plasma treatment are collected in Table 3.1. The flow rate values in the Table 3.1 are the volumetric flow rates in the plasma source inlet. Samples 1 and 2 were exposed only to the D/Ne plasma, while samples 3 and 4 passed two-step plasma treatment (Table 3.1). The aim of the first step was to modify the sample surface in a way which is favorable for D retention. During the second step the structures produced at the surface were loaded by deuterium. According to [65] the retention drastically decreases with the temperature growth. This is the reason why during this step the surface temperature was kept low.

In case of the D/Ne plasma the particles' flux density was approximately 10^{24} m^{-2} s^{-1} and in case of D plasma it was nearly 20 times lower. The value of the target bias voltage was -40 V.

Table 3.1. Plasma regimes

Sample	Coating	Plasma & total exposition	Field, T	FWHM mm	Plasma current, A	Peak temp, °C	D flow rate, slm	Ne flow rate, slm
1	W	D_2/Ne; 600 s	0.8	12	50–60	1300	0.7	2.22
2	W/Y							
3	W	D_2/Ne; 300 s	0.8	12	50–60	1300	0.7	2.22
4	W/Y	+D_2; 300 s	0.4	25	10–15	< 600	2.5	0

During the plasma exposure a spectral pyrometer and an IR camera were used for recording of the temperature at the sample surface.

To estimate the gross erosion profile, fast visible light camera with the interference filter for W I spectral line at 400.9 nm (bandwith less than 2 nm) was used. The frame rate and the exposure time of the camera were 100 Hz and 9.9 ms, respectively. In addition, to estimate the proportion of continuous background in the camera signal, spectra from different points at the sample surface were recorded in 20 nm region centered at the W 400.9 nm line using the Czerny-Turner spectrometer with the 300 lines/mm grating.

The LIBS setup is described in the part considering Magnum-PSI and Pilot-PSI (2.1.2 Figure 2.2).

Flux of D/Ne plasma causes an intensive erosion of the sample material accompanied by the radiation of W 400.9 nm line (Figure 3.15 a). In case of D plasma flux the radiation originated from the sample surface was not detectable.

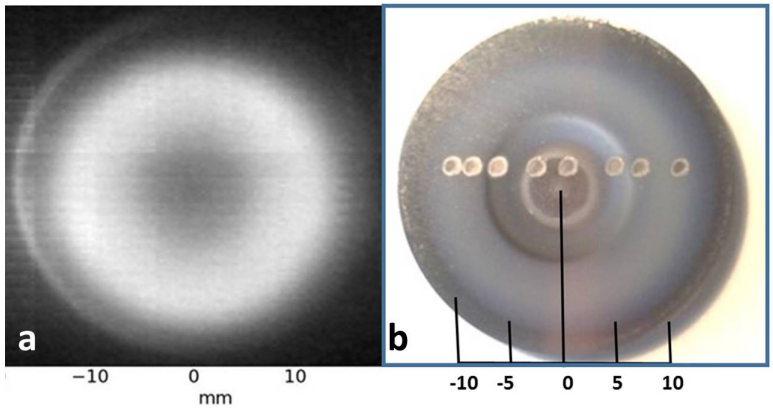

Figure 3.15. a) W radiation near 400.9 nm wavelength recorded during D/Ne plasma flux b) due to the plasma action ring-like pattern is formed at the sample surface. Row of round spots are craters formed during LIBS measurements.

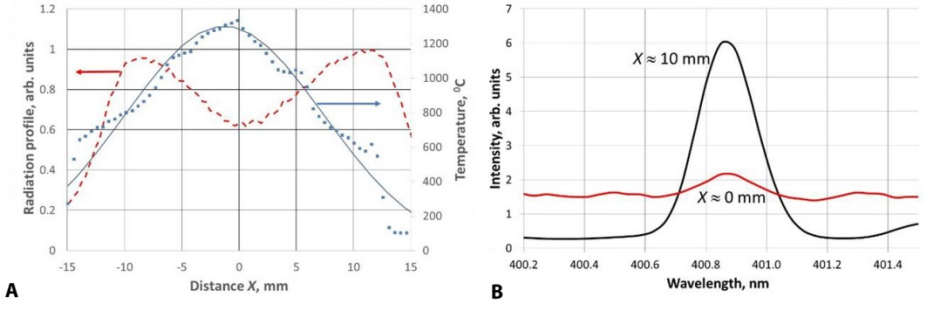

Figure 3.16. Sample 1, D/Ne plasma. a) dots – temperature distribution along the sample diameter; solid line – Gaussian fit with FWHM = 12.25 mm; dashed line – radiation profile recorded by 400.9 nm interference filter. b) the spectrum near 400.9 nm at the center and at the edge of a sample.

Keeping in mind that the erosion is caused mainly by Ne ions, Figures 3.15a, 3.16a show that the Ne ions hit the outer circular region with the flux maximum at $X \approx 10$ mm. Radiation recorded with the 400.9 nm filter is the sum of a continuous spectrum and the W line. According to Figure 3.16b it is possible to say that at the sample center the W radiation had a very low intensity and thus the amount of the sputtered material was small. At the same time from the temperature profile (Figure 3.16a) follows that the maximum of the energy

delivered by plasma flux is at the sample center. Such uneven distribution of charged particles at the sample surface is confirmed by recent probe studies [48]: depending on the bias voltage of sample, in linear plasma machines the plasma flux can bombard the sample with electrons in the central region and with ions in the remaining part. SEM pictures (Figure 3.17) demonstrate that the ring-like pattern at the plasma-exposed sample (Figure 3.15b) reflects the morphology differences along the sample surface.

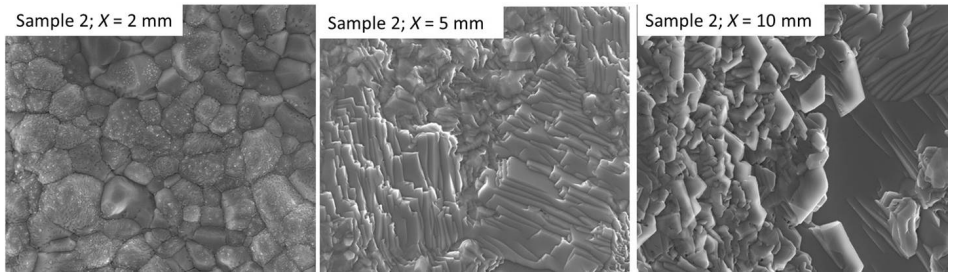

Figure 3.17. Sample 2. SEM pictures at different distances *X*.

In spite of different coatings compositions and plasma fluxes directed to the samples, for all samples the main regularities of the surface structure are the same. At the central part of samples, the surface has a grain–like structure which at outer parts is replaced by a plate-like structure (Figure 3.17). At distances $8 \le X \le 11$ mm the surface had an increased roughness.

The LIBS spectra where recorded from different parts at the sample surface. It should be pointed that LIBS results reflect the net erosion while the distribution in Fig 3.15a is related to gross erosion.

Each crater in Figure 3.15b is formed by 100 laser shots. Spectral lines which had an acceptable signal-to noise ratio in 420–490 nm spectral range, are presented in Table 3.2.

Tabel 3.2. Detected W and Mo spectral lines

Element	Wavelength, nm	g_kA_{ki}, s^{-1}	E_k, eV
W I	465.987	3.00E+06	2.66
W I*	468.761	1.33E+07	5.03
W I	484.381	9.50E+06	2.97
Mo I	470.726	3.27e+08	5.12
Mo I*	473.144	4.98E+08	5.22
Mo I	476.019	6.07E+08	5.25
Mo I	481.925	2.44E+08	5.2
Mo I	483.051	2.85E+08	5.2
Mo I	486.800	1.56E+08	5.14

To build elemental depth profiles we chose spectral lines belonging to transitions, which upper state energies E_u had close values: for W 468.761 nm and Mo 473.144 nm lines the E_u values are 5.03 and 5.22 eV, respectively. As a rough estimation, it was supposed that the populations of these states $x_k = I_{ki}/g_k A_{ki}$ are proportional to the concentration of species. Thus, the relative concentrations r_{Mo} and r_W good be found as $r_{W,Mo} = \frac{x_{W,Mo}}{x_W + x_{Mo}}$.

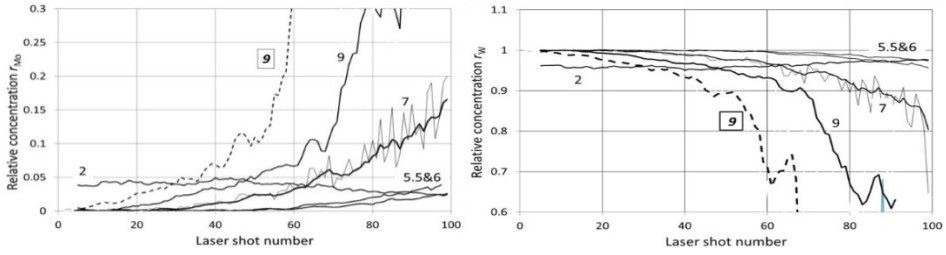

Figure 3.18. W/Y coating. LIBS profiles for Mo (A) and for W (B), figures are distances from the sample center in mm. Thinner lines (X = 7 mm) are the results without smoothing, thicker lines present the moving average over 4 points. Dashed lines are sample 2 (W coating) profiles at X = 9 mm.

Assuming that the ablation rate is independent of the position X, from Figure 3.18 follows that the thickness of the W layer is thinnest at $X \approx 10$ mm and the thickness gradually decreased towards center. This result matches with the trend observed in the case of gross erosion (Figure 3.15 a, Figure 3.16) i.e. after the plasma exposure the remained W layer is thinner at places where the gross erosion is larger. From the comparison of the depth profiles for W/Y and W coatings at X = 9 mm follows that Y increased the persistence of the coating to plasma fluxes.

At the central part of samples, we see the presence of Mo starting from the first laser shot. This is the reason why the value of r_W at the center is lower than it is at X = 5 mm. Besides, remarkable is that at the sample center both r_W and r_{Mo} values remain practically unchanged during 100 laser shots i.e. due to the Ne/D plasma flux an efficient mixing of W and Mo took place. It is hard to explain these findings only by erosion/deposition processes at the sample surface. As in the previous measurements (3.2.1, [II]) it could be possible that the Mo originates from the plasma source or from the Mo clamping ring and due to the high value of temperature the mixing of W and Mo take place.

SIMS results presented in Figure 3.19 are raw dependences i.e. they show how the concentration of an element changes with depth but they do not allow comparing the W and Mo relative concentrations. SIMS supports the LIBS findings. Indeed, at X = 9 mm the W coating is the thinnest and it gradually

increases towards center. At the same time the Mo signal follows the same trend and in the central part it is close to its maximum value. Dashed lines in Figure 3.19 demonstrate the effect of plasma exposure time. According to Table 3.1, for sample 4 the exposure time to Ne/D plasma is two times shorter and the thickness of the remaining W layer at X = 5 mm is ≈ 1.5 times bigger. From the comparison of SIMS and LIBS profiles the laser ablation rate value for the W/Y coating is ≈ 10 nm per shot.

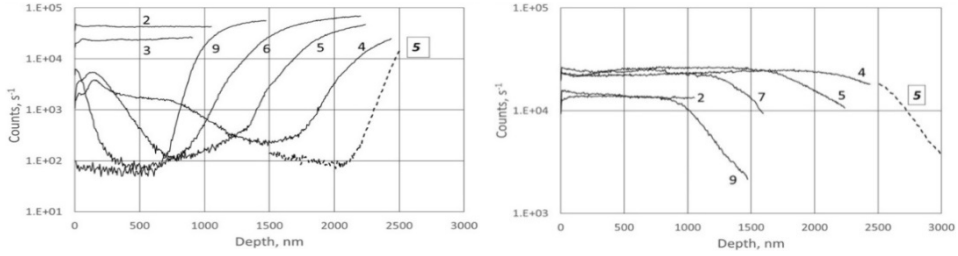

Figure 3.19. Mo (left) and W (right) SIMS profiles; parameter – distance (mm) from the center; dashed lines – sample 4 profiles at 5 mm distance from the center.

In Figure 3.20 Balmer D_α -line and H_α -line were fitted with Lorentzian contours (FWHM = 0.14 nm). At X = 9 mm the deuterium is detectable during the first five laser shots while at X = 2 mm the intensity of the D_α -line is at the noise level. This result confirms that the retention is more efficient in places of increased surface roughness. Intensity of H_α -line remains practically independent of the laser shot number, likely it is caused by the presence of water vapor in background Ar gas. Again, these LIBS results match with those obtained by SIMS where at 100 nm depth the D_α -line intensity at the sample center was more by an order lower then at ≈ 10 mm distance.

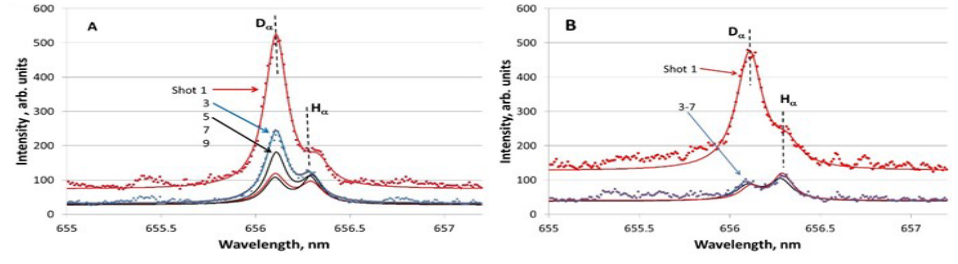

Figure 3.20. Sample 4(W/Y coating). Spectra at distances X = 9 mm (A) X = 2 mm (B) for different laser shots. Dots – experiment; solid lines – Lorentzian fit. Spectra were recorded in Ar at 1.2 mbar background pressure.

Profiles obtained by ion μ-beam PIXE measurements for Mo, W and D concentration along the sample surface are presented in Figure 3.21. Results for the Mo and W show good correspondence to the results obtained by LIBS and SIMS. Mo concentration is highest at the center, once again referring to Mo deposition from the plasma source or the clamping ring used. Also some Mo is detected approximately 10 mm from the center. W distribution is more uniform, having minima in the locations with higher Mo concentration. The distribution of D concentration, measured by μ-beam, has some contradictions with the LIBS results. Namely, μ-beam shows maximum of D concentration approximately 4 mm from the center, meanwhile for LIBS measurements the most persistent signal was measured 9 mm from the center. Reason for this effect is not clear. One possible reason is ageing of the samples: μ-beam measurements were carried out more than half a year after the LIBS experiments. Possible outgassing during the experiments should be also considered in the further studies. Uneven distribution of D in the W, described in [66], may also affect the profiles. NRA measurements revealed that maximum D concentration for the samples was around $2.5 \cdot 10^{16}$ cm^2.

In this study W coatings with and without Y doping were exposed to D and Ne plasma in the linear plasma device Pilot-PSI. Several *in-situ* (LIBS, IR thermography, spectral pyrometer, optical emission imaging) and *post-mortem* (SEM, SIMS, μ-beam PIXE, NRA) were applied to characterize the samples. The results confirmed that the erosion of W coatings was caused by Ne ions. D loading to the samples is most effective at low surface temperature (<600 ^oC) and in the regions with increased roughness (plated structure is present). Y doping of a few atomic percent reduces the sputtering yield of W coatings remarkably. We demonstrated that LIBS is a reliable *in-situ* technique for characterizing erosion and deposition processes on W coatings and gives results that coincide reasonably with the ones obtained by SIMS. At 1.2 mbar Ar background pressure Balmer D_α -line signal was reliable detected and resolved from the H_α -line. LIBS enabled to describe the D retention gradients along the sample surface. Nevertheless, further study is needed to achieve quantitative results.

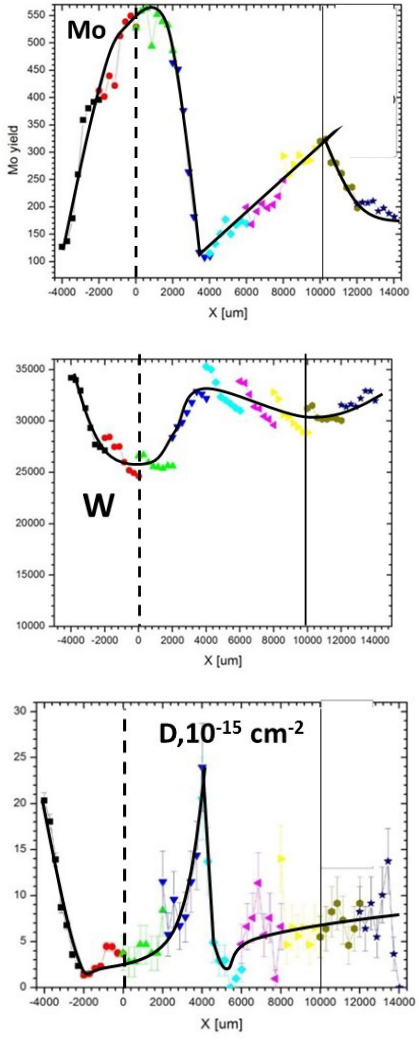

Figure 3.21. Sample 4(W/Y coating); Elements' distribution along sample diameter. PIXE by ^{3}He beam and NRA analyses.

SUMMARY (MAIN RESULTS)

In this work laser-induced breakdown spectroscopy (LIBS) applicability for on-line monitoring of ITER-relevant materials at low background pressure (from 10^{-6} mbar to 2 mbar) was investigated.

Post-mortem experiments were carried out on domestic LIBS device equipped with Nd:YAG laser lasing at 1064 nm, 532 nm and 266 nm. Minimal residual pressure was 10^{-6} mbar. Single-shot spectra were recorded in a wide spectral range (280 – 850 nm) with the echelle spectrometer and Czerny-Turner spectrometer was used for recording in a selected 20 nm range. Spectrometers were equipped with time-gated ICCD cameras.

As a first step, the regularities of the development of the laser-produced tungsten (W) plasma plume were investigated. ICCD images confirmed that at low pressure (10^{-3} mbar) the plasma plume expansion is diffusive. At 1.8 mbar Ar background pressure a clearly distinguishable front is formed. 200 ns after the laser plume the plume expansion had reached 5 mm and 3 mm from the target at 10^{-3} mbar and 2 mbar, respectively. 100 ns after the laser pulse the velocity of the plasma plume at 1 mbar and 10^{-3} mbar was 8 km/s and 15 km/s, respectively. Afterwards the velocity decreased linearly. On that base appropriate experimental parameters were selected. At low pressure (less than 10^{-3} mbar) optimal time gate and delay time for tungsten LIBS measurements were found to be around 100 ns and 500 ns, respectively. Laser fluence ensuring reasonable compromise between spectra signal-to-noise ratio and the ablation rate for pure W coatings was found to be around 7 J/cm^2.

For application of calibration-free LIBS a set of W spectral lines were tested in the 400–443 nm spectral range. It appeared that the most intensive W lines (400.88 nm, 407.44 nm, 429.46 nm) are influenced by strong self-absorption and they are not applicable for the calibration-free LIBS measurements. It was found that during the first 400 ns the electron temperature changed from 1.25 to 0.65 eV. In addition, the dependence of electron temperature and signal-to-noise ratio for the W spectral lines on laser wavelength (266 nm and 1064 nm) was studied. At 10^{-3} mbar pressure the electron temperature was independent of laser wavelength but at 266 nm the value of the signal-to-noise ratio was larger.

In case of the composite layers aluminum (Al) was used as a proxy for beryllium. The ablation rate of W/Al coatings was strongly dependent on the aluminum content. For pure tungsten coatings the minimal ablation rate corresponding to LIBS spectra with reasonable signal-to-noise ratio was less than 100 nm per laser pulse. While for the Al-containing (up to 40 at. %) the corresponding ablation rate was remarkably higher (up to 400 nm per laser pulse).

In addition to the sample composition the surface morphology of the tested samples had a strong effect on the recorded LIBS spectra. Ablation rate for W samples with porous structure was up to 10 times higher compared to the smooth samples.

It was shown that in most cases background pressure in the range of 1 mbar is needed for detecting D from pure W tungsten coatings (tests on Asdex Upgrade tokamak divertor tiles and *in-situ* measurements on Pilot-PSI linear plasma device). As an exception, for the W/Al coating the deuterium signal was detectable also at low (10^{-6} mbar) pressure. Optimal delay time for deuterium detection was 150 – 200 ns and optimal fluence was somewhat lower from the one suggested for measuring tungsten spectral lines. Analyzing samples exposed to tokamak-relevant plasma (in Asdex Uprade tokamak or linear plasma devices Magnum-PSI and Pilot-PSI) it was shown that LIBS could be applied for erosion, deposition and deuterium retention measurements.

To test *in-situ* LIBS applicability for real tokamak-like conditions, experiments were carried out on Magnum-PSI and Pilot-PSI linear plasma devices. Samples were exposed to He, D_2 and neon plasma fluxes. In case of Magnum-PSI device the LIBS spectra were recorded in the target exchange and analyzes chamber, while in Pilot-PSI case the measurements were carried out in "true" *in-situ* conditions. In addition to *in-situ* LIBS measurements other *in-situ* (IR thermography, spectral pyrometer, optical emission imaging) and *post-mortem* (SEM, SIMS, μ-beam, NRA) techniques were applied to characterize the samples. The LIBS results match reasonably well with those obtained by other methods. LIBS allowed the resolving of the deuterium and hydrogen Balmer α-lines at 1.2 mbar Ar background pressure. A clear dependence of the deuterium retention on the surface structures was demonstrated. Retention was much higher in plated structures than in the regions with smooth surface.

To sum up, in this study the preliminary experiments needed to apply LIBS as a quantitative *in-situ* tool for monitoring tungsten-containing layers erosion in ITER were carried out: the optimal parameters for the spectral recording and suitable spectral lines are suggested; the influence of the sample composition and surface morphology to the LIBS spectra was described. The ablation rate per laser pulse that determines the precision of these measurements was in the limits of 20–400 nm, depending on the surface morphology and sample composition. Deuterium and hydrogen lines were spectrally resolved and at least qualitatively reliable *in-situ* measurements of deuterium retention were carried out in linear plasma device Pilot-PSI.

OPEN PROBLEMS AND SUGGESTIONS FOR THE FURTHER RESEARCH

On the basis of the present study arose a number of problems and research questions to be solved before applying LIBS as an *in-situ* tool for erosion, deposition and fuel retention study in tokamaks:

1. A quantitative model or calibration database is needed to find the ablation rate from the parameters of LIBS spectra. For further information systematic experimental and possibly modeling studies are needed.
2. Self-absorption correction coefficients are needed for tungsten spectral lines to apply calibration-free LIBS approach for tungsten containing samples. Direct measurements of absorption coefficients in tungsten plasma plume are needed.
3. In this work deuterium and hydrogen lines were spectrally resolved. For tokamak applications study on tritium containing samples is essential. To resolve deuterium and tritium spectral lines, a LIBS recording setup with sufficient spectral resolution and meanwhile with good sensitivity has to be designed. In addition to that the optimal recording options (delay time, time gate, background pressure, laser pulse parameters) have to be figured out. Experiments with tritium containing samples have to be performed.
4. Methodology to determine absolute deuterium and tritium concentrations (instead of relative concentrations) is needed. This is needed to estimate the amount of fuel (deuterium and tritium) in the ITER walls. The main concern is the amount of tritium that is considered as an important safety issue. One possible approach is absolute intensity measurements. In this case the ionization degree of the plasma has to be known to convert the spectral line intensity to the number of particles.

SUMMARY IN ESTONIAN

In-situ LIBSi rakendamine ITERisse sobilike materjalide uurimiseks

Kontrollitud tuumasünteesil on võrreldes traditsiooniliste energiaallikatega mitmeid eeliseid. Selle energialiigi kasutuselevõtuks on ehitamisel eksperimentaalne tuumasünteesireaktor ITER (ingl ***I**nternational **T**hermonuclear **E**xperimental **R**eactor*), mis on läbi aegade suurimaid teadusprojekte. Üheks lõpuni lahendamata probleemiks on reaktori seinte seiramine plasmalahenduste vahel. Reaktori tõrgeteta toimimise tagamiseks on vajalik jälgida erosiooni- ja sadestumisprotsesse ning kütuse (deuteeriumi ja triitiumi) salvestumist seadme seintesse. Üheks võimalikuks seiremeetodiks on laser-indutseeritud plasma spektroskoopia (LIBS).

Töös uuriti LIBS rakendatavust ITERisse sobilike materjalide *in-situ* ekspressanalüüsiks madalal (kuni 2 mbar) taustrõhul. Peamiseks uuritavaks materjaliks oli volfram (W) ja selle segud alumiiniumiga (Al). Alumiiniumi kasutati ITERis kasutatava berülliumi (Be) asemel, kuna Be on toksiline ning selle uurimine ei ole enamikus laborites võimalik. Samuti uuriti deuteeriumi (D) detekteerimise ning deuteeriumi ja vesiniku (H) spektrijoonte eraldamise küsimusi.

Töö esimeses osas antakse lühike teoreetiline ülevaade LIBSist, LIBSi rakendamise spetsiifikast ITERisse sobivate materjalide ning tingimuste jaoks ning plasma-tahkise vastastikmõju uurimise hetkeseisust.

Töö teises osas tutvustatakse kasutatud eksperimendiseadmeid: kodulabori LIBS seadet, lineaarseid plasmamasinaid Pilot-PSI ja Magnum-PSI ning neile üles seatud *in-situ* LIBS süsteemi. Lühidalt kirjeldatakse ka kasutatud proove ning nende karakteriseerimiseks kasutatud analüüsimeetodeid.

Kolmandas osas kirjeldatakse töö tulemusi. Töösse lisatud artiklites avaldatud tulemustest antakse lühiülevaade, seni publitseerimata tulemusi tutvustatakse pikemalt.

Post-mortem analüüsid teostati Nd:YAG laseriga (lainepikkused 1064, 532 ja 266 nm) LIBS seadmel. LIBS spekter salvestati Echelle spektromeetriga laias piirkonnas (280–850 nm) ja Czerny-Turner spektromeeter 20 nm laiuses eelvalitud piirkonnas. Mõlemad spektromeetrid olid varustatud ajalise lahutusega valgusvõimendiga digitaalkaameratega (ICCD).

Esimese sammuna uuriti W laser-indutseeritud plasma levikut. Madalal rõhul (10^{-3} mbar) on plasmatombu levik difuusne. Kõrgemal rõhul (2 mbar) moodustub ruumis leviva plasmatombu selge esifront. 200 ns pärast laservälget ulatus plasmatomp rõhkudel 10^{-3} mbar ja 1.8 mbar vastavalt 5 ja 3 mm kaugusele märklauast. 100 ns pärast laservälget oli tombu liikumise kiirus 8 km/s (1.8 mbar) ja 15 km/s (10^{-3} mbar). Hiljem see kahanes ligikaudu lineaarselt. Leiti, et madalal rõhul (alla 10^{-3} mbar) on spektri salvestamist optimaalne alustada 100 ns pärast laservälget. Säriaja optimaalne pikkus on 500 ns ja energia pindtihedus 5 J/cm^2.

Kalibratsioonivaba LIBSi rakendamiseks uuriti W spektrijooni piirkonnas 400–443 nm. Selgus, et intensiivsemad spektrijooned (400,88 nm; 407,44 nm ja 429,49 nm) on omaneeldumisest tugevalt mõjutatud. Esimese 400 ns jooksul vähenes Boltzmanni diagrammidelt leitud elektrontemperatuur 1,25 elektronvoldilt 0,65 elektronvoldile. Lisaks uuriti signaal-müra suhte ning elektrontemperatuuri sõltuvust laseri lainepikkusest (kasutati lainepikkusi 266 nm ja 1064 nm). Elektrontemperatuur lainepikkusest ei sõltunud, kuid signaal-müra suhe oli enamike joonte jaoks suurem lainepikkusel 266 nm.

W/Al katete ablatsioonikiiruse uurimisel selgus, et Al osakaal kattes mõjutas ablatsioonikiirust märkimisväärselt. Puhta W korral oli mõistliku signaal-müra suhtega spektrit võimalik salvestada ka ablatsioonikiirusel alla 100 nm laservälke kohta. Al sisaldusega (kuni 40 %) oli vastav ablatsioonikiirus oluliselt suurem (kuni 400 nm laservälke kohta).

Lisaks proovide koostisele mõjutas ablatsioonikiirust ning salvestatud LIBS spektreid tugevalt ka pinna morfoloogia. Poorsete struktuuride puhul oli ablatsioonikiirus võrreldes siledate katetega kuni kümme korda suurem.

Selgus, et puhtast W valmistatud katetest (tokamaki ASDEX Upgrade divertori proovid ja *in-situ* mõõtmised lineaarsel plasmaseadmel Pilot-PSI) D detekteerimiseks LIBSi abil on enamasti vajalik 1 mbar suurusjärgus taustrõhk. W/Al segust koosnevatest katetest õnnestus D detekteerida ka madalal rõhul (10^{-6} mbar). Optimaalne viiteaeg deuteeriumi detekteerimiseks oli 150-200 ns ning energia pindtihedus oli veidi madalam sellest, mida kasutati W spektrijoonte mõõtmiseks.

Uurimaks LIBSi rakendatavust *in-situ* mõõtmisteks reaalsesse tokamaki sobilikes tingimustes, teostati mõõtmised lineaarsetel plasmaseadmetel Magnum-PSI ja Pilot-PSI (Hollandis DIFFER instituudis). Proove eksponeeriti heeliumi, deuteeriumi ja neooni plasmaga. Magnum-PSI mõõtmised teostati eksperimendid spetsiaalses proovide vahetamise ning analüüsimise kambris. Pilot-PSI puhul teostati tõelised *in-situ* mõõtmised. Lisaks LIBSile kasutati proovide karakteriseerimiseks teisi meetodeid: infrapunatermograafia, püromeetria, skaneeriv elektronmikroskoopia, sekundaarsete ioonide mass-spektroskoopia, tuumareaktsioonide analüüs). LIBSi ja teiste meetodite tulemused olid heas vastavuses. 1,2 mbar Ar taustrõhu juures õnnestus Balmeri seeria D_α ja H_α spekterijooned edukalt spektraalselt lahutada. Mõõtmised näitasid, et proovis salvestunud deuteeriumi kogus sõltub tugevalt proovi pinna struktuurist. Plaatja struktuuriga piirkondades oli deuteeriumi kontsentratsioon märgatavalt kõrgem kui sileda pinna puhul.

Kokkuvõtvalt tehti eeltöö, mis on vajalik kvantitatiivse *in-situ* LIBSi rakendamiseks volframit sisaldavate proovide erosiooni mõõtmiseks ITERis: selgitati välja optimaalsed parameetrid spektri salvestamiseks ning sobivad spektrijooned, kirjeldati proovide koostise ning pinna morfoloogia mõju proovide koostisele. Ablatsioonikiirus laservälke kohta, mis määrab erosiooni mõõtmise täpsuse, oli sõltuvalt proovi koostisest ja pinna morfoloogiast vahemikus 20–400 nm. Lineaarsel plasmaseadmel Pilot-PSI viidi läbi kvalitatiivsed *in-situ*

LIBS mõõtmised, mis kirjeldasid salvestunud deuteeriumi kogust volframkatetes.

Sellest hoolimata on küsimusi, mis vajavad edasist uurimist. Usaldusväärsete sügavusprofiilide leidmiseks tuleb süstemaatiliselt uurida seoseid LIBS spektri ning proovi ablatsioonikiiruse vahel. Kalibratsioonivaba LIBS metodoloogia kasutamiseks on tarvis põhjalikult uurida W joonte omaneeldumist. Võimalusi korral tuleb leida vastavad koefitsiendid paranduste sisseviimiseks. LIBSi rakendamisel tuumasünteesi reaktori seintesse salvestunud kütuse hulga määramiseks tuleb spektraalselt lahutada deuteeriumi ja triitiumi jooned, mille lainepikkused on veelgi lähedasemad kui selles töös kasutatud deuteeriumi ja vesiniku spektrijoontel. Selleks tuleb läbi viia katsed triitiumi sisaldavate proovidega ning leida optimaalselt mõõtmisparameetrid. Lisaks tuleb leida metodoloogia deuteeriumi ning triitiumi absoluutsete kontsentratsioonide määramiseks LIBS spektrist.

ACKNOWLEDGEMENTS

First of all I would like to thank my supervisors Associate Professor Matti Laan and Dr. Peeter Paris for the help during my studies.

I would like to thank the staff of the Gas Discharge Laboratory for the useful advice and technical solutions.

I wish to thank Dr. Hennie van der Meiden and his colleagues in FOM Institute DIFFER for the great support they provided during my experiments on linear plasma devices.

Finally, my greatest thanks to my family.

REFERENCES

[1] J. Freidberg "*Plasma Physics and Fusion Energy*" Cambridge University Press (2008)

[2] V. Philipps, A. Malaquias, A. Hakola "Development of laser-based techniques for in situ characterization of the first wall in ITER and future fusion devices" *Nucl. Fusion*, **53**, 9, 093002 (2013)

[3] Reinhard Noll "*Laser-Induced Breakdown Spectroscopy"* Springer (2012)

[4] J. P. Singh and S. N. Thakur "*Laser-Induced Breakdown Spectroscopy*" Elsevier (2007)

[5] G. Colonna, A. Casavola and, M. Capitelli "Modelling of LIBS plasma expansion" *Spectrohim. Acta Part B*, **56**, 567–586 (2001)

[6] L. I. Sedov "*Similarily and dimensional methods in Mechanics*" CRC press (1993)

[7] V. K. Unnikrishnan, R. Nayak, K. Aithal "Analysis of trace elements in complex matrices (soil) by Laser Induced Breakdown Spectroscopy (LIBS)" *Anal. Meth.*, **5**, 1294–1300 (2013)

[8] P. Paris, M. Aints, A. Hakola "Determination of elemental depth profiles by multi-spot averaging technique of LIBS spectra" *Fusion Eng. and Design*, **86**, 6–8, 1125–1128 (2011)

[9] C. Lopez-Moreno, K. Amponsah-Manager, B. W. Smith "Quantitative analysis of low-alloy steel by microchip laser induced breakdown spectroscopy" *J. Anal. At. Spectros.* **20**, 552–556 (2005)

[10] L. Xu, V. Bulatov, V. V. Gridin and, I. Schechter "Absolute Analysis of Particulate Materials by Laser-Induced Breakdown Spectroscopy" *Anal. Chem.*, **69**, 11, 2103–2108 (1997)

[11] M. P. Mateo, G. Nicolas, V. Pinon and A. Yanez "Improvements in depth-profiling of thick samples by laser-induced breakdown spectroscopy using linear correlation" *Surface and Interface Anal.*, 3**8**, 941–948 (2006)

[12] T. Hussain and M. A. Gondal "Laser induced breakdown spectroscopy (LIBS) as a rapid tool for material analysis" *J. Phys.: Conference Series*, **439**, 012050 (2013)

[13] E. Tognoni, G. Cristoforetti, S. Legnaioli, and, V. Palleschi "Calibration-Free Laser-Induced Breakdown Spectroscopy: State of the art" *Spectrochim. Acta Part B*, **65**, 1–14 (2010)

[14] G. Cristoforetti, A. De Giacomob, M. Dell'Aglio "Local Thermodynamic Equilibrium in Laser-Induced Breakdown Spectroscopy: Beyond the McWhirter criterion" *Spectrochim. Acta Part B: At. Spectros.*, **65**, 1, 86–95 (2010)

[15] M. A. Ismail, H. Imam, A. Elhassan, W. T. Youniss, and M. A. Harith "LIBS limit of detection and plasma parameters of some elements in two different metallic matrices" *J. Anal. At. Spectrom.*, **19**, 489–494 (2004)

[16] S. Rai, A. K. Rai, S. N. Thakur "Identification of nitro-compounds with LIBS" *Appl. Phys. B*, **19**, 645–650 (2008)

[17] A. Khumaeni, T. Motonobu, A. Katsuaki "Enhancement of LIBS emission using antenna-coupled microwave" *Opt. Express*, **21**, 24, 29755–29768 (2013)

[18] A.M. El Sherbini, Th. M. El Sherbini, Hegazy "Evaluation of self-absorption coefficients of aluminum emission lines in laser-induced breakdown spectroscopy measurements" *Spectrohim Acta Part B*, **60**, 1573–1579 (2005)

[19] J. L. Craston, R. Hancox, A. E. Robson "The role of materials in controlled thermonuclear research" *Geneva Conference on Peaceful Uses of Atomic Energy*, P/34, 414–426 (1958).

[20] G. M. McCracken and P.E. Stott "Plasma-surface interactions in tokamaks" *Nucl. Fusion*, **19**, 7, 889–979 (1979)
[21] S.S. Khirwadkar, K. P. Singh, Y.Patil "Fabrication and characterization of tungsten and graphite based PFC for divertor target elements of ITER like tokamak application" *Fusion Eng. and Design*, **86**, 9–11, 1736–1740 (2011)
[22] S. Brezinsek, JET-EFDA contributors "Plasma-surface interaction in the Be/W environment: Conclusions drawn from the JET-ILW for ITER" *J. Nucl. Mater.*, **463**, 11–21 (2015)
[23] V. A. Makhlaj, I. E. Garkusha, S. V. Malykhin "Residual stresses in tungsten under exposures with ITER ELM-like plasma loads" *Phys. Scr*., **T138**, 014060 (2009)
[24] J. Roth, E. Tsitrone, T. Loarer "Tritium inventory in ITER plasma-facing materials and tritium removal procedures" *Plasma Phys. Control. Fusion,* **50** 103001 (2008)
[25] T. Hirai, G. Pintsuk, J. Linke, M. Batilliot "Cracking failure study of ITER-reference tungsten grade under single pulse thermal shock loads at elevated temperatures" *J. Nucl. Mater.,* **390–391**, 751–754 (2009)
[26] G. De Temmerman, K. Bystrov, R. P. Doerner "Helium effects on tungsten under fusion-relevant plasma loading conditions" *J. Nucl. Mater.*, **438**, S78–S83 (2013)
[27] Y. Ueda, H.Y. Peng, H.T. Lee "Helium effects on tungsten surface morphology and deuterium retention" *J. Nucl. Mater.,* **442,** S267–S272 (2013)
[28] J. Linke, T. Loewenhoff, V. Massaut "Performance of different tungsten grades under transient thermal loads" *Nucl. Fusion,* **51**, 073017 (2011)
[29] M. Wirtz, J. Linke, G. Pintsuk **"**Comparison of thermal shock damages induced by different simulation methods on tungsten" *J. Nucl. Mater.,* **438**, S833–S836 (2013)
[30] R. Mitteau, R. Eatona, G. Perez "Status of the beryllium tile bonding qualification activities for the manufacturing of the ITER first wall" *Fusion Eng. and Design*, **88–89**, 1367–1370 (2015)
[31] V. Philipps, P. Mertens, G.F. Matthews, H. Maier, JET-EFDA contributors "Overview of the JET ITER-like Wall Project" *Fusion Eng. and Design,* **85**, 7–9, 1581–1586 (2010)
[32] R.P. Doerner, C. Björkas, D. Nishijima and, T. Schwarz-Selingerd "Erosion of beryllium under high-flux plasma impact" *J. Nucl. Mater.,* **438**, S272–S275 (2013)
[33] S. Carpentier, R.A. Pitts and, P.C. Stangeby "Modelling of beryllium erosion–redeposition on ITER first wall panels" *J. Nucl. Mater.,* **415**, 1, S165–S169 (2011)
[34] L. Marot, C. Linsmeier, B. Eren, L. Moser, R. Steiner, E. Meyer "Can aluminium or magnesium be a surrogate for beryllium: A critical investigation of their chemistry" *Fusion Eng. and Design*, **88**, 1718–1721 (2013)
[35] D. W. Hahn and N. Omenetto "Laser-Induced Breakdown Spectroscopy (LIBS), Part I: Review of Basic Diagnostics and Plasma–Particle Interactions: Still-Challenging Issues Within the Analytical Plasma Community", *Appl. Spectros*., **64**, 12, 335A–366A (2010)
[36] D. W. Hahn and N. Omenetto "Laser-Induced Breakdown Spectroscopy (LIBS), Part II: Review of Instrumental and Methodological Approaches to Material Analysis and Applications to Different Fields" *Appl. Spectros.*, **66**, Issue 4, 347–419 (2012)

[37] A. Huber, B .Schweer, V. Philipps “Study of the feasibility of applying laser-induced breakdown spectroscopy for *in-situ* characterization of deposited layers in fusion devices” *Phys. Scr.*, **T145**, 014028 (2011)
[38] J. Karhunen, A. Hakola, J. Likonen, A. Lissovski, M. Laan, P. Paris, JET EFDA Contributors “Applicability of LIBS for *in situ* monitoring of deposition and retention on the ITER-like wall of JET – Comparison to SIMS” *J. Nucl. Mater.*, **463**, 931–935 (2015)
[39] M. Pribula, J. Karhunen, P. Paris “Determination of deuterium depth profiles in fusion-relevant wall materials by nanosecond LIBS” Abstract submitted to *22nd International Conference on Plasma Surface Interactions in Controlled Fusion Devices*
[40] A.M. El Sherbini, H. Hegazy, T. M. El Sherbini “Measurement of electron density utilizing the Hα-line from laser produced plasma in air” *Spectrochim. Acta Part B: At. Spectros.*, **61**, 5, 532–539 (2006)
[41] L. Mercadier, J. Hermann, C. Grisolia and, A. Semerok “Plume segregation observed in hydrogen and deuterium containing plasmas produced by laser ablation of carbon fiber tiles from a fusion reactor” *Spectrochim. Acta Part B: At. Spectros.*, **65**, 8, 715–720 (2010)
[42] Louis St-Onge “A mathematical framework for modeling the compositional depth profiles obtained by pulsed laser ablation”, *J. Anal. At. Spectrom.*, **17**, 1083–1089 (2002)
[43] FOM Institute DIFFER PSI-Facilities and Instrumentation http://www.differ.nl/research/fusion/psi-facilities-and-instrumentation/facilities last visited 10.03.16
[44] W. A. J. Vijvers, D. C. Schram, A. E. Shumack “Experimental and theoretical determination of the efficiency of a sub-atmospheric flowing high power cascaded arc hydrogen plasma source” *Plasma Sources Sci. Tech.*, **19**, 6, 065016 (2010)
[45] J. J. Zielinski “A high power pulsed plasma system for material testing under simultaneous continuous and transient loads” PhD thesis, FOM Institute DIFFER, The Netherlands (2013)
[46] A. E. Shumack, V. P. Veremiyenko, D. C. Schram “Rotation of a strongly magnetized hydrogen plasma column determined from an asymmetric Balmer-β spectral line with two radiating distributions” *Phys. Rev. E*, **78**, 046405 (2008)
[47] A. E. Shumack, H. J. de Blank, J. Westerhout and G. J. van Rooij “Two-dimensional electric current effects on a magnetized plasma in contact with a surface” *Plasma Phys. and Controlled Fusion*, **54**, 125006 (2012)
[48] C. Costin, V. Anita, F. Ghiorghiu “Cross-section analysis of the Magnum-PSI plasma beam using a 2D multi-probe system” *Plasma sources Sci. and Tech,.* **24**, 015014 (2015)
[49] M.A. van den Berg, S. Brons, O.G. Kruijt “The target for the new plasma/wall experiment Magnum-PSI” *Fusion Eng. and Design*, **86**, 1745–1748 (2011)
[50] H. J. van der Meiden “Thomson scattering on low and high temperature plasmas” PhD thesis, FOM institute DIFFER, The Netherlands (2011)
[51] P. Paris, A. Hakola, K. Bystrov “Erosion of marker coatings exposed to Pilot-PSI plasma” *J. Nucl. Mater.,* **438**, S754–S757 (2013)
[52] S. Lehto, J. Likonen, J.P. Coad “Tungsten coating on JET divertor tiles for erosion/deposition studies” *Fusion Eng. Design*, **66–68**, 241–245 (2003)
[53] N. Lemahieu, J. Linke, G. Pintsuk “Performance of yttrium doped tungsten under 'edge localized mode'-like loading conditions”*Phys. Scr.*,**T159**, 014035 (2014)

[54] V. Tiron, I-L. Velicu, O. Vasilovici "HiPIMS technique used for fusion related mixed materials" *published poster presentation*, 33nd ICPIG, July 26–31, Iași, Romania (2015)
[55] S. S. Harilal, C. V. Bindhu, M. S. Tillack "Internal structure and expansion dynamics of laser ablation plumes into ambient gases" *J. Appl. Phys.*, **93**, 2380 (2003)
[56] N. Farid, C. Li, H. Wang and, Hongbin Ding "Laser-induced breakdown spectroscopic characterization of tungsten plasma using the first, second, and third harmonics of an Nd:YAG laser" *J. Nucl. Mater.*, **433**, 1–3, 80–85 (2013)
[57] L. A. Álvarez-Trujillo, A. Ferrero, J. J. Laserna and, D. W. Hahn "Alternative Statistical Methods for Spectral Data Processing: Applications to Laser-Induced Breakdown Spectroscopy of Gaseous and Aerosol Systems" *Appl. Spec.*, **62**, 1144–1152 (2008)
[58] 2015 EUROfusion Work Package PFC SP 5.2 Report, 2014, University of Tartu
[59] A.Hakola "WP PFC SP5: Post mortem analyses and material migration", Joint Annual Meeting of JET2 and PFC, *oral presentation*, Culham, 23–26 November 2015
[60] C. C. Tang and D. W. Hess "Plasma-enhanced chemical vapor deposition of β-tungsten, a metastable phase" *Appl. Phys. Lett.*, **45**, 6, 633–635 (1984)
[61] 2014 EUROfusion Work Package PFC SP 5.2 Report, 2014, University of Tartu
[62] S. Kajita, T. Saeki, N. Yoshida, N. Ohno, and A. Iwamae "Nanostructured Black Metal: Novel Fabrication Method by Use of Self-Growing Helium Bubbles" *Appl. Phys. Express,* **3,** 085204 (2010)]
[63] G. De Temmerman, M.A. van den Berg, J. Scholten "High heat flux capabilities of the Magnum-PSI linear plasma device" *Fusion Eng. and Design,***88***,* 483–487 (2013)
[64] D. Naujoks, K. Asmussen, M. Bessenrodt-Weberpals "Tungsten as target material in fusion devices" *Nucl. Fusion*, **36**, 6, 671–687 (1996)
[65] V. K. Alimov, B. Tyburska-Püschel, S. Lindig, Y. Hatano "Temperature dependence of surface morphology and deuterium retention in polycrystalline ITER-grade tungsten exposed to low-energy, high-flux D plasma" *J. Nucl. Mater.,* **420**, 1–3, 519–524 (2012)
[66] H. Bergsåker, I. Bykov, P. Petersson "Microscopically nonuniform deposition and deuterium retention in the divertor in JET with ITER-like wall" *J. Nucl. Mater.*, **463,** 956–960 (2015)

PUBLICATIONS

CURRICULUM VITAE

Name: Kaarel Piip
Date of birth: June 8, 1987, Tartu, Estonia
Nationality: Estonian
Address: W. Ostwaldi 1, Tartu, 50411
Phone: +372 737 4676
+372 55 90 7949
E-mail: kaarel.piip@ut.ee

Education:

2012	University of Tartu, MsC *cum laud*e (physics)
2010	University of Tartu, BsC *cum laude* (physics)
2006	Hugo Treffneri Gümnaasium

Language:
Estonian
English

Research Activity:
1. Main research topics:
Laser-induced breakdown spectroscopy, plasma-surface interaction

2. List of the publications included in the thesis

[I] Lissovski, A.; **Piip, K**.; Hämarik, L.; Aints, M.; Laan, M.; Paris, P.; Hakola, A.; Karhunen, J. (2015). LIBS for tungsten diagnostics in vacuum: Selection of analytes. *Journal of Nuclear Materials*, 463, 923–926

[II] **Piip, K**.; De Temmerman, G.; van der Meiden, H.J.; Lissovski, A; Karhunen, J.; Aints, M.; Hakola, A.; Paris, P.; Laan, M.; Likonen, J.; Jõgi, I.; Kozlova, J.; Mändar, H. (2015). LIBS analysis of tungsten coatings exposed to Magnum PSI ELM-like plasma. Journal of Nuclear Materials, 463, 919–922,

[III] **Piip, K**.; Paris, P.; Hakola, A.; Bystrov, K.; De Temmerman, G.; Aints, M.; Jõgi, I.; Kozlova, J.; Laan, M.; Likonen, J.; Lissovski, A.; Mändar, H. (2014). Influence of He/D_2 plasma fluxes on the morphology and crystallinity of tungsten coatings. Physica Scripta, 89 (4), nr 044009

[IV] Paris, P.; **Piip, K**.; Hakola, A.; Laan, M.; Aints, M.; Koivuranta, S.; Likonen, J.; Lissovski, A.; Mayer, M.; Neu, N.; Rohde, V.; Sugiyama, K. (2015). Development of laser induced breakdown spectroscopy for studying erosion, deposition, and fuel retention in ASDEX Upgrade. Fusion Engineering and Design, 98–99, 1349–1352

3. Other related publications

[a] Karhunen, J.; Hakola, A.; Likonen, J.; Lissovski, A.; Paris, P.; Laan, M.; **Piip, K**.; Porosnicu, C.; Lungu, C. P.; Sugiyama, K. (2014). Development

of laser-induced breakdown spectroscopy for analyzing deposited layers in ITER. Physica Scripta, 2014, 014067

[b] Van der Meiden, H.; Berg, M.; Brons, S.; Ding, H.; Eck, H.; Hoen, M.; Karhunen, J.; Kruif, T.; Laan, M.; Li, C.; Lissovski, A.; Morgan, T.; Paris, P.; **Piip, K.**; Pol, M.; Scannell, R.; Scholten, J.; Smeets, P.; Spork, C.; Emmichoven, P. ... De Temmerman, G. (2013). Laser-based diagnostics applications for plasma-surface interaction studies. Journal of Instrumentation, 8, 1−14,

[c] **Piip, K**.; Van der Meiden, H. J.; Hämarik, L.; Karhunen, J.; Hakola, A.; Paris, P.; Aints, M.; Laan, M.; Likonen, J.; Bystrov, K.; Kozlova, J.; Kanarbik, R. (2015). In situ LIBS in the linear plasma device Pilot-PSI for Fusion Application. *15th International Conference on Plasma Facing Materials & Components for Fusion Applications, Aix-en-Provence, 18-22 May, 2015.* 75−75, book of abstracts

[d] **Piip, K**.; Paris, P.; Hakola, A.; Bystrov, K.; De Temmerman, G.; Aints, M.; Jõgi, I.; Kozlova, J.; Laan, M.; Likonen, J.; Lissovski, A. (2013). Influence of He/D_2 plasma fluxes on tungsten marker coatings. *In: 14th International Conference on Plasma-Facing Materials and Components for Fusion Applications Book of Abstracts: 14th International Conference on Plasma-Facing Materials and Components for Fusion Applications, Juelich, Germany, 13–17 May 2013,* book of abstarcts

[e] **Piip, K.**; Laan, M.; Paris, P.; Aints, M.; Hakola, A.; Karhunen, J.; Likonen, J.; Lissovski, A.; Petersson, P.; Rubel, M. (2013). First wall monitoring by LIBS: options and limitations. *In: Europhysics Conference Abstracts: 40th EPS Conference on Plasma Physics; Finland Espoo; 1–5 July.* (37D), book of abastracts

ELULOOKIRJELDUS

Nimi: Kaarel Piip
Sünniaeg: 8. juuni 1987, Tartu, Eesti
Kodakondus: Eesti
Aadress: W. Ostwaldi 1, Tartu, 50411
Telefon: +372 737 4676
+372 55 90 7949
E-post: kaarel.piip@ut.ee

Haridus:

2012	Tartu Ülikool, magistrikraad *cum laud*e (füüsika)
2010	University of Tartu, bakalaureusekreed *cum laude* (füüsika)
2006	Hugo Treffneri Gümnaasium

Keelteoskus:
eesti
inglise

Teadustegevus:
1. Peamised uurimisvaldkonnad:
Laser-indutseeritud plasma spektroskoopia, plasma ja tahkise vastastikmõju

2. Dissertatsiooni lsiatud publikatsioonid

[I] Lissovski, A.; **Piip, K**.; Hämarik, L.; Aints, M.; Laan, M.; Paris, P.; Hakola, A.; Karhunen, J. (2015). LIBS for tungsten diagnostics in vacuum: Selection of analytes. *Journal of Nuclear Materials*, 463, 923–926

[II] **Piip, K**.; De Temmerman, G.; van der Meiden, H.J.; Lissovski, A; Karhunen, J.; Aints, M.; Hakola, A.; Paris, P.; Laan, M.; Likonen, J.; Jõgi, I.; Kozlova, J.; Mändar, H. (2015). LIBS analysis of tungsten coatings exposed to Magnum PSI ELM-like plasma. Journal of Nuclear Materials, 463, 919–922,

[III] **Piip, K**.; Paris, P.; Hakola, A.; Bystrov, K.; De Temmerman, G.; Aints, M.; Jõgi, I.; Kozlova, J.; Laan, M.; Likonen, J.; Lissovski, A.; Mändar, H. (2014). Influence of He/D_2 plasma fluxes on the morphology and crystallinity of tungsten coatings. Physica Scripta, 89 (4), nr 044009

[IV] Paris, P.; **Piip, K**.; Hakola, A.; Laan, M.; Aints, M.; Koivuranta, S.; Likonen, J.; Lissovski, A.; Mayer, M.; Neu, N.; Rohde, V.; Sugiyama, K. (2015). Development of laser induced breakdown spectroscopy for studying erosion, deposition, and fuel retention in ASDEX Upgrade. Fusion Engineering and Design, 98–99, 1349–1352

3. Teised seotud publikatsioonid

[a] Karhunen, J.; Hakola, A.; Likonen, J.; Lissovski, A.; Paris, P.; Laan, M.; **Piip, K**.; Porosnicu, C.; Lungu, C. P.; Sugiyama, K. (2014). Development of laser-induced breakdown spectroscopy for analyzing deposited layers in ITER. Physica Scripta, 2014, 014067

[b] Van der Meiden, H.; Berg, M.; Brons, S.; Ding, H.; Eck, H.; Hoen, M.; Karhunen, J.; Kruif, T.; Laan, M.; Li, C.; Lissovski, A.; Morgan, T.; Paris, P.; **Piip, K.**; Pol, M.; Scannell, R.; Scholten, J.; Smeets, P.; Spork, C.; Emmichoven, P. ... De Temmerman, G. (2013). Laser-based diagnostics applications for plasma-surface interaction studies. Journal of Instrumentation, 8, 1–14,

[c] **Piip, K**.; Van der Meiden, H. J.; Hämarik, L.; Karhunen, J.; Hakola, A.; Paris, P.; Aints, M.; Laan, M.; Likonen, J.; Bystrov, K.; Kozlova, J.; Kanarbik, R. (2015). In situ LIBS in the linear plasma device Pilot-PSI for Fusion Application. *15th International Conference on Plasma Facing Materials & Components for Fusion Applications,* Aix-en-Provence, Prantsusmaa*,* 18.–22. mai 2015*,*, abstraktide kogu

[d] **Piip, K**.; Paris, P.; Hakola, A.; Bystrov, K.; De Temmerman, G.; Aints, M.; Jõgi, I.; Kozlova, J.; Laan, M.; Likonen, J.; Lissovski, A. (2013). Influence of He/D_2 plasma fluxes on tungsten marker coatings. *14th International Conference on Plasma-Facing Materials and Components for Fusion Applications,* Saksamaa*,* 13.–17. mai 2013*,* abstraktide kogu

[e] **Piip, K.**; Laan, M.; Paris, P.; Aints, M.; Hakola, A.; Karhunen, J.; Likonen, J.; Lissovski, A.; Petersson, P.; Rubel, M. (2013). First wall monitoring by LIBS: options and limitations. *Europhysics Conference Abstracts: 40th EPS Conference on Plasma Physics;* Espoo, Soome, 1.–5. juuli 2013, (37D), abstraktide kogu

DISSERTATIONES PHYSICAE UNIVERSITATIS TARTUENSIS

1. **Andrus Ausmees.** XUV-induced electron emission and electron-phonon interaction in alkali halides. Tartu, 1991.
2. **Heiki Sõnajalg.** Shaping and recalling of light pulses by optical elements based on spectral hole burning. Tartu, 1991.
3. **Sergei Savihhin.** Ultrafast dynamics of F-centers and bound excitons from picosecond spectroscopy data. Tartu, 1991.
4. **Ergo Nõmmiste.** Leelishalogeniidide röntgenelektronemissioon kiiritamisel footonitega energiaga 70–140 eV. Tartu, 1991.
5. **Margus Rätsep.** Spectral gratings and their relaxation in some low-temperature impurity-doped glasses and crystals. Tartu, 1991.
6. **Tõnu Pullerits.** Primary energy transfer in photosynthesis. Model calculations. Tartu, 1991.
7. **Olev Saks.** Attoampri diapasoonis voolude mõõtmise füüsikalised alused. Tartu, 1991.
8. **Andres Virro.** AlGaAsSb/GaSb heterostructure injection lasers. Tartu, 1991.
9. **Hans Korge.** Investigation of negative point discharge in pure nitrogen at atmospheric pressure. Tartu, 1992.
10. **Jüri Maksimov.** Nonlinear generation of laser VUV radiation for high-resolution spectroscopy. Tartu, 1992.
11. **Mark Aizengendler.** Photostimulated transformation of aggregate defects and spectral hole burning in a neutron-irradiated sapphire. Tartu, 1992.
12. **Hele Siimon.** Atomic layer molecular beam epitaxy of A^2B^6 compounds described on the basis of kinetic equations model. Tartu, 1992.
13. **Tõnu Reinot.** The kinetics of polariton luminescence, energy transfer and relaxation in anthracene. Tartu, 1992.
14. **Toomas Rõõm.** Paramagnetic H^{2-} and F^+ centers in CaO crystals: spectra, relaxation and recombination luminescence. Tallinn, 1993.
15. **Erko Jalviste.** Laser spectroscopy of some jet-cooled organic molecules. Tartu, 1993.
16. **Alvo Aabloo.** Studies of crystalline celluloses using potential energy calculations. Tartu, 1994.
17. **Peeter Paris.** Initiation of corona pulses. Tartu, 1994.
18. **Павел Рубин.** Локальные дефектные состояния в CuO_2 плоскостях высокотемпературных сверхпроводников. Тарту, 1994.
19. **Olavi Ollikainen.** Applications of persistent spectral hole burning in ultrafast optical neural networks, time-resolved spectroscopy and holographic interferometry. Tartu, 1996.
20. **Ülo Mets.** Methodological aspects of fluorescence correlation spectroscopy. Tartu, 1996.
21. **Mikhail Danilkin.** Interaction of intrinsic and impurity defects in CaS:Eu luminophors. Tartu, 1997.

22. **Ирина Кудрявцева.** Создание и стабилизация дефектов в кристаллах KBr, KCl, RbCl при облучении ВУФ-радиацией. Тарту, 1997.
23. **Andres Osvet.** Photochromic properties of radiation-induced defects in diamond. Tartu, 1998.
24. **Jüri Örd.** Classical and quantum aspects of geodesic multiplication. Tartu, 1998.
25. **Priit Sarv.** High resolution solid-state NMR studies of zeolites. Tartu, 1998.
26. **Сергей Долгов.** Электронные возбуждения и дефектообразование в некоторых оксидах металлов. Тарту, 1998.
27. **Kaupo Kukli.** Atomic layer deposition of artificially structured dielectric materials. Tartu, 1999.
28. **Ivo Heinmaa.** Nuclear resonance studies of local structure in $RBa_2Cu_3O_{6+x}$ compounds. Tartu, 1999.
29. **Aleksander Shelkan.** Hole states in CuO_2 planes of high temperature superconducting materials. Tartu, 1999.
30. **Dmitri Nevedrov.** Nonlinear effects in quantum lattices. Tartu, 1999.
31. **Rein Ruus.** Collapse of 3d (4f) orbitals in 2p (3d) excited configurations and its effect on the x-ray and electron spectra. Tartu, 1999.
32. **Valter Zazubovich.** Local relaxation in incommensurate and glassy solids studied by Spectral Hole Burning. Tartu, 1999.
33. **Indrek Reimand.** Picosecond dynamics of optical excitations in GaAs and other excitonic systems. Tartu, 2000.
34. **Vladimir Babin.** Spectroscopy of exciton states in some halide macro- and nanocrystals. Tartu, 2001.
35. **Toomas Plank.** Positive corona at combined DC and AC voltage. Tartu, 2001.
36. **Kristjan Leiger.** Pressure-induced effects in inhomogeneous spectra of doped solids. Tartu, 2002.
37. **Helle Kaasik.** Nonperturbative theory of multiphonon vibrational relaxation and nonradiative transitions. Tartu, 2002.
38. **Tõnu Laas.** Propagation of waves in curved spacetimes. Tartu, 2002.
39. **Rünno Lõhmus.** Application of novel hybrid methods in SPM studies of nanostructural materials. Tartu, 2002.
40. **Kaido Reivelt.** Optical implementation of propagation-invariant pulsed free-space wave fields. Tartu, 2003.
41. **Heiki Kasemägi.** The effect of nanoparticle additives on lithium-ion mobility in a polymer electrolyte. Tartu, 2003.
42. **Villu Repän.** Low current mode of negative corona. Tartu, 2004.
43. **Алексей Котлов.** Оксианионные диэлектрические кристаллы: зонная структура и электронные возбуждения. Tartu, 2004.
44. **Jaak Talts.** Continuous non-invasive blood pressure measurement: comparative and methodological studies of the differential servo-oscillometric method. Tartu, 2004.
45. **Margus Saal.** Studies of pre-big bang and braneworld cosmology. Tartu, 2004.

46. **Eduard Gerškevitš.** Dose to bone marrow and leukaemia risk in external beam radiotherapy of prostate cancer. Tartu, 2005.
47. **Sergey Shchemelyov.** Sum-frequency generation and multiphoton ionization in xenon under excitation by conical laser beams. Tartu, 2006.
48. **Valter Kiisk.** Optical investigation of metal-oxide thin films. Tartu, 2006.
49. **Jaan Aarik.** Atomic layer deposition of titanium, zirconium and hafnium dioxides: growth mechanisms and properties of thin films. Tartu, 2007.
50. **Astrid Rekker.** Colored-noise-controlled anomalous transport and phase transitions in complex systems. Tartu, 2007.
51. **Andres Punning.** Electromechanical characterization of ionic polymer-metal composite sensing actuators. Tartu, 2007.
52. **Indrek Jõgi.** Conduction mechanisms in thin atomic layer deposited films containing TiO_2. Tartu, 2007.
53. **Aleksei Krasnikov.** Luminescence and defects creation processes in lead tungstate crystals. Tartu, 2007.
54. **Küllike Rägo.** Superconducting properties of MgB_2 in a scenario with intra- and interband pairing channels. Tartu, 2008.
55. **Els Heinsalu.** Normal and anomalously slow diffusion under external fields. Tartu, 2008.
56. **Kuno Kooser.** Soft x-ray induced radiative and nonradiative core-hole decay processes in thin films and solids. Tartu, 2008.
57. **Vadim Boltrushko.** Theory of vibronic transitions with strong nonlinear vibronic interaction in solids. Tartu, 2008.
58. **Andi Hektor.** Neutrino Physics beyond the Standard Model. Tartu, 2008.
59. **Raavo Josepson.** Photoinduced field-assisted electron emission into gases. Tartu, 2008.
60. **Martti Pärs.** Study of spontaneous and photoinduced processes in molecular solids using high-resolution optical spectroscopy. Tartu, 2008.
61. **Kristjan Kannike.** Implications of neutrino masses. Tartu, 2008.
62. **Vigen Issahhanjan.** Hole and interstitial centres in radiation-resistant MgO single crystals. Tartu, 2008.
63. **Veera Krasnenko.** Computational modeling of fluorescent proteins. Tartu, 2008.
64. **Mait Müntel.** Detection of doubly charged higgs boson in the CMS detector. Tartu, 2008.
65. **Kalle Kepler.** Optimisation of patient doses and image quality in diagnostic radiology. Tartu, 2009.
66. **Jüri Raud.** Study of negative glow and positive column regions of capillary HF discharge. Tartu, 2009.
67. **Sven Lange.** Spectroscopic and phase-stabilisation properties of pure and rare-earth ions activated ZrO_2 and HfO_2. Tartu, 2010.
68. **Aarne Kasikov.** Optical characterization of inhomogeneous thin films. Tartu, 2010.
69. **Heli Valtna-Lukner.** Superluminally propagating localized optical pulses. Tartu, 2010.

70. **Artjom Vargunin.** Stochastic and deterministic features of ordering in the systems with a phase transition. Tartu, 2010.
71. **Hannes Liivat.** Probing new physics in e+e− annihilations into heavy particles via spin orientation effects. Tartu, 2010.
72. **Tanel Mullari.** On the second order relativistic deviation equation and its applications. Tartu, 2010.
73. **Aleksandr Lissovski.** Pulsed high-pressure discharge in argon: spectroscopic diagnostics, modeling and development. Tartu, 2010.
74. **Aile Tamm.** Atomic layer deposition of high-permittivity insulators from cyclopentadienyl-based precursors. Tartu, 2010.
75. **Janek Uin.** Electrical separation for generating standard aerosols in a wide particle size range. Tartu, 2011.
76. **Svetlana Ganina.** Hajusandmetega ülesanded kui üks võimalus füüsikaõppe efektiivsuse tõstmiseks. Tartu, 2011
77. **Joel Kuusk.** Measurement of top-of-canopy spectral reflectance of forests for developing vegetation radiative transfer models. Tartu, 2011.
78. **Raul Rammula**. Atomic layer deposition of HfO_2 – nucleation, growth and structure development of thin films. Tartu, 2011.
79. **Сергей Наконечный.** Исследование электронно-дырочных и интерстициал-вакансионных процессов в монокристаллах MgO и LiF методами термоактивационной спектроскопии. Тарту, 2011.
80. **Niina Voropajeva.** Elementary excitations near the boundary of a strongly correlated crystal. Tartu, 2011.
81. **Martin Timusk.** Development and characterization of hybrid electro-optical materials. Tartu, 2012, 106 p.
82. **Merle Lust.** Assessment of dose components to Estonian population. Tartu, 2012, 84 p.
83. **Karl Kruusamäe.** Deformation-dependent electrode impedance of ionic electromechanically active polymers. Tartu, 2012, 128 p.
84. **Liis Rebane.** Measurement of the $W \to \tau\nu$ cross section and a search for a doubly charged Higgs boson decaying to τ-leptons with the CMS detector. Tartu, 2012, 156 p.
85. **Jevgeni Šablonin.** Processes of structural defect creation in pure and doped MgO and NaCl single crystals under condition of low or super high density of electronic excitations. Tartu, 2013, 145 p.
86. **Riho Vendt**. Combined method for establishment and dissemination of the international temperature scale. Tartu, 2013, 108 p.
87. **Peeter Piksarv.** Spatiotemporal characterization of diffractive and non-diffractive light pulses. Tartu, 2013, 156 p.
88. **Anna Šugai.** Creation of structural defects under superhigh-dense irradiation of wide-gap metal oxides. Tartu, 2013, 108 p.
89. **Ivar Kuusik.** Soft X-ray spectroscopy of insulators. Tartu, 2013, 113 p.
90. **Viktor Vabson**. Measurement uncertainty in Estonian Standard Laboratory for Mass. Tartu, 2013, 134 p.

91. **Kaupo Voormansik.** X-band synthetic aperture radar applications for environmental monitoring. Tartu, 2014, 117 p.
92. **Deivid Pugal.** hp-FEM model of IPMC deformation. Tartu, 2014, 143 p.
93. **Siim Pikker.** Modification in the emission and spectral shape of photostable fluorophores by nanometallic structures. Tartu, 2014, 98 p.
94. **Mihkel Pajusalu**. Localized Photosynthetic Excitons. Tartu, 2014, 183 p.
95. **Taavi Vaikjärv.** Consideration of non-adiabaticity of the Pseudo-Jahn-Teller effect: contribution of phonons. Tartu, 2014, 129 p.
96. **Martin Vilbaste.** Uncertainty sources and analysis methods in realizing SI units of air humidity in Estonia. Tartu, 2014, 111 p.
97. **Mihkel Rähn.** Experimental nanophotonics: single-photon sources- and nanofiber-related studies. Tartu, 2015, 107 p.
98. **Raul Laasner.** Excited state dynamics under high excitation densities in tungstates. Tartu, 2015, 125 p.
99. **Andris Slavinskis.** EST Cube-1 attitude determination. Tartu, 2015, 104 p.
100. **Karlis Zalite**. Radar Remote Sensing for Monitoring Forest Floods and Agricultural Grasslands. Tartu, 2016, 124 p.